

The Impact of Cooling and Feedback on Disc Galaxies

Frank C. van den Bosch

Max-Planck Institut für Astrophysik, Karl Schwarzschild Str. 1, Postfach 1317, 85741 Garching, Germany

ABSTRACT

In the standard picture of galaxy formation mass and angular momentum are the two main parameters that determine the properties of disc galaxies. The details of how the gas inside dark matter haloes is transformed into a luminous disc, however, depend strongly on the physics of star formation, feedback and cooling, which are poorly understood. The efficiencies of these astrophysical processes are ultimately responsible for setting the galaxy mass fractions f_{gal} defined as the ratio of galaxy mass (disc plus bulge) to total virial mass. Therefore, if we could somehow determine $f_{\text{gal}}(M_{\text{vir}})$ from observations of the luminous component of disc galaxies, this would allow us to put stringent constraints on the efficiencies of cooling and feedback. This, however, requires estimating the total virial mass, which is a delicate problem. In this paper we use detailed, analytical models for the formation of disc galaxies to investigate the impact that cooling and feedback have on their structural properties. In particular, we investigate which observables extracted directly from the models are best suited as virial mass estimators, and to what extent they allow the recovery of the model input parameters regarding the feedback and cooling efficiencies. Contrary to naive expectations, the luminosities and circular velocities of disc galaxies are extremely poor indicators of total virial mass. Instead, we show that the product of disc scale length and rotation velocity squared yields a much more robust virial mass estimate, which allows a fairly accurate recovery of the galaxy mass fractions as function of virial mass. We also show that feedback can cause a narrow correlation between f_{gal} and the halo spin parameter, as recently found by van den Bosch, Burkert & Swaters from an analysis of dwarf galaxy rotation curves. Finally we investigate the impact that cooling and feedback have on the colors, metallicities, star formation histories and Tully-Fisher relation of disc galaxies.

Key words: galaxies: formation — galaxies: fundamental parameters — galaxies: kinematics and dynamics — galaxies: structure — dark matter.

1 INTRODUCTION

Currently, the main uncertainties in our picture of galaxy formation are related to the intricate processes of cooling, star formation, and feedback. In particular, we need to understand how efficient feedback is in expelling baryons from dark matter haloes, and how it enriches the IGM. This in turn influences the cooling efficiencies, which influences the subsequent star formation rates, which influences the subsequent amount of energy that is fed back into the IGM, etc. The importance of this complicated loop of ‘gastrophysics’ has long been realized. Already the first detailed models of galaxy formation by White & Rees (1978) revealed an important problem intrinsic to any hierarchical formation scenario in which small mass clumps merge to form larger and larger structures. At early times, collapsed objects have much higher densities, and therefore much shorter cooling times than at the present time. Consequently, when these objects merge to form larger and larger structures (i.e., galax-

ies and clusters), the vast majority of their baryons have already cooled, so that by the present time there is basically no gas left to make up the intergalactic or intra-cluster medium observed throughout the Universe. This problem has become known as the ‘cooling catastrophe’ and is generally interpreted as a requirement for some sort of feedback mechanism that can pump energy back into the gas to lower its cooling efficiency (see Balogh et al. 2001 for an overview of the current status).

In the past, two related techniques have been used to investigate the impact of cooling and feedback on galaxy formation: numerical simulations (e.g., Katz, Weinberg & Hernquist 1996; Fardal et al. 2001; Pearce et al. 2000; Kay et al. 2001), and semi-analytical modeling (e.g., Kauffmann, White & Guiderdoni 1993; Somerville & Primack 1999; Cole et al. 2000). In both cases phenomenological prescriptions are used to describe star formation and feedback, and the resulting model galaxies are compared to observational data.

However, an important problem is that so far none of these models have been able to successfully fit all observables. This is likely to be a consequence of the simplicity of the phenomenological descriptions used. An additional problem is that assumptions have to be made about poorly constrained model ingredients such as stellar populations, the stellar initial mass function, dust extinction, etc. Often the ignorance regarding these ingredients is hidden in free model parameters, which have hampered the model's ability to place direct, stringent constraints on the efficiencies of cooling and feedback. Finally, the galaxy models are poorly (in the case of numerical simulations) or not at all (in the case of most semi-analytical models) spatially resolved, which can complicate a direct comparison with observations.

In this paper we therefore take a slightly different approach based on new models for the formation of disc galaxies that are both spatially and temporally resolved. Rather than comparing the models to actual observations of real disc galaxies (which is postponed to future papers), we investigate how well observables *extracted directly from the models* can be used to *recover* the input parameters of the model regarding the feedback and cooling efficiencies. This has the advantage that even though the assumptions underlying the model are not necessarily correct, and the phenomenological descriptions of star formation and feedback are certainly oversimplified, it provides important insights regarding the ability to use actual observations to constrain the poorly understood astrophysical processes of galaxy formation. The main goal of this paper is therefore not to tune our models to best fit data, but to investigate how both cooling and feedback impact on the observable properties of the model galaxies.

The cooling and feedback efficiencies are ultimately responsible for setting the galaxy mass fractions $f_{\text{gal}} = M_{\text{gal}}/M_{\text{vir}}$. Here M_{gal} is the total *baryonic* mass of the galaxy (stars plus gas, excluding the hot gas in the halo). Ideally one would therefore like to observationally obtain some measure of f_{gal} as function of virial mass. The main focus in this paper, therefore, is to investigate how well one can hope to recover $f_{\text{gal}}(M_{\text{vir}})$ from direct observations of the population of galaxies. Unfortunately, obtaining a measure of f_{gal} for a single galaxy faces two important challenges. First of all we need to be able to infer the total baryonic mass from observations, which requires a conversion of luminosities and HI and CO masses to stellar, atomic and molecular masses, respectively. The appropriate conversion ratios, however, are still relatively uncertain. Even more problematic is inferring the total virial mass from the photometry and kinematics of the luminous component. An important focus of this paper, therefore, is to identify those observables that are best suited as indicators of both M_{gal} and M_{vir} .

After introducing the models (Section 2), we discuss one particular model galaxy in detail to illustrate the characteristics of the models (Section 3). In Section 4 we explore how cooling and feedback impact on the galaxy mass fractions, and we search for the observables that are best suited to recover the model input parameters. In Sections 5 and 6 we discuss the impact of cooling and feedback on the Tully-Fisher relation, and on the star formation rates, colors and metallicities of disc galaxies, respectively. We summarize our results in Section 7.

2 THE MODELS

The model for the formation of disc galaxies used here is presented in van den Bosch (2001; hereafter paper 1). Here we give a short overview of the main ingredients of the model, and we refer the interested reader to Paper 1 for a more detailed description.

The main assumptions that characterize the framework of our models are the following: (i) dark matter halos around disc galaxies grow by the smooth accretion of mass, (ii) in the absence of cooling the baryons have the same distribution of mass and angular momentum as the dark matter, and (iii) the baryons conserve their specific angular momentum when they cool.

The two main ingredients that determine the formation and evolution of a disc galaxy, therefore, are (the evolution of) the mass and angular momentum of the virialized object; $M_{\text{vir}}(r, z)$ and $J_{\text{vir}}(r, z)^*$. We characterize the angular momentum of the protogalaxies by the dimensionless spin parameter $\lambda = J_{\text{vir}}|E_{\text{vir}}|^{1/2}G^{-1}M_{\text{vir}}^{-5/2}$. Here E_{vir} is the halo's energy, and G is the gravitational constant. We follow Firmani & Avila-Reese (2000) and make the additional assumptions that (iv) the spin parameter λ of a given galaxy is constant with time, (v) each mass shell that virializes is in solid body rotation, and (vi) the rotation axes of all shells are aligned. Although neither of these assumptions is necessarily accurate, it was shown in Paper 1 that they result in halos with angular momentum profiles that are in excellent agreement with the high resolution N -body simulations of Bullock et al. (2001b).

The main outline of the models is as follows. We set up a radial grid between $r = 0$ and the present day virial radius of the model galaxy and we follow the formation and evolution of the disc galaxy using a few hundred time steps. We consider six mass components: dark matter, hot gas, disc mass (both in stars and in cold gas), bulge mass, and mass ejected by outflows from the disc. The dark matter, hot gas, and bulge mass are assumed to be distributed in spherical shells, whereas the disc stars and cold gas are assumed to be in infinitesimally thin annuli. Each time step we compute the changes in these various mass components in each radial bin, using the prescriptions detailed below.

2.1 The evolution of the dark matter component

The backbone of the models is the formation and evolution of the dark matter haloes, which is determined by the parameters of the background cosmological model and by the power spectrum $P(k)$ of the initial density fluctuations. In this paper we restrict ourselves to the currently popular Λ CDM model with $\Omega_0 = 0.3$, $\Omega_\Lambda = 0.7$, and $H_0 = 100h \text{ km s}^{-1} \text{ Mpc}^{-1}$ with $h = 0.7$. We adopt the standard CDM power spectrum normalized to $\sigma_8 = 1.0$ and we use a baryon density of $\Omega_{\text{bar}} = 0.019h^{-2}$ (Tytler et al. 1999).

The rate at which dark matter haloes grow in mass depends on cosmology and halo mass, and can be computed using extended Press-Schechter theory (Bond et al. 1991; Lacey & Cole 1993; Sheth & Tormen 1999). In Figure 1

* Throughout this paper, r and z refer to spherical radius and redshift, respectively.

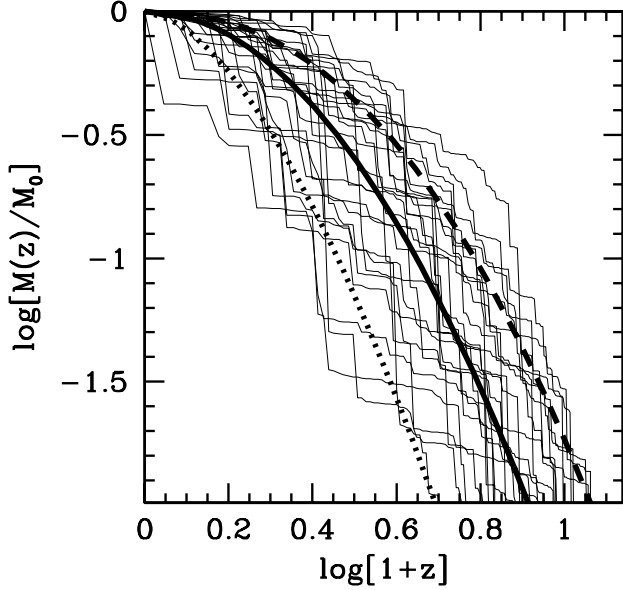


Figure 1. Thin lines correspond to 25 randomly selected MAHs for a $5 \times 10^{11} h^{-1} M_{\odot}$ halo in our standard Λ CDM Universe, constructed using the method described in van den Bosch (2002). The thick solid line corresponds to the universal MAH (equation [1]), and provides an accurate description of the average MAH for haloes of this mass. The dashed and dotted lines correspond to the early and late MAHs described in the text (Section 3.1), respectively, and roughly outline the distribution of MAHs for a halo of this mass. They are parameterized by the universal MAHs for halo masses of $2 \times 10^9 h^{-1} M_{\odot}$ and $10^{14} h^{-1} M_{\odot}$ respectively.

we plot 25 random realizations of mass accretion histories (hereafter MAH) of a halo with present day mass $M_{\text{vir}}(0) = 5 \times 10^{11} h^{-1} M_{\odot}$ in the Λ CDM cosmology adopted here (thin lines). These MAHs are constructed using the method outlined in van den Bosch (2002). The thick solid line corresponds to the average MAH of a $5 \times 10^{11} h^{-1} M_{\odot}$ halo (averaged over a large ensemble of MAHs), which is well fitted by the universal form:

$$\log \left(\frac{M_{\text{vir}}(z)}{M_{\text{vir}}(0)} \right) = -0.301 \left[\frac{\log(1+z)}{\log(1+z_f)} \right]^{\nu} \quad (1)$$

(van den Bosch 2002). Here $M_{\text{vir}}(z)$ is the virial mass at redshift z , z_f is the redshift at which the halo mass is half the present day mass, and

$$\nu = 1.211 + 1.858 \log[1+z_f] + 0.308 \Omega_{\Lambda}^2 - 0.032 \log[M_{\text{vir}}(0)/(10^{11} h^{-1} M_{\odot})] \quad (2)$$

The ‘formation’ redshift z_f depends on halo mass and cosmology and is easily computed using the Press-Schechter formalism (see Appendix in van den Bosch 2002). Throughout this paper we use this ‘universal’ MAH, and which is valid for all halo masses and for a wide variety of cosmologies, to describe the rate at which dark matter haloes grow in mass. Each model galaxy is therefore to be regarded as averaged over all its possible MAHs.

We assume that the dark matter virializes such that at each redshift the halo is spherical with a NFW (Navarro, Frenk & White 1997) density distribution:

$$\rho_{\text{vir}}(r) = \rho_s \left(\frac{r}{r_s} \right)^{-1} \left(1 + \frac{r}{r_s} \right)^{-2}. \quad (3)$$

We parameterize each dark matter halo by its total virial mass M_{vir} and its concentration parameter $c = r_{\text{vir}}/r_s$. Here the virial radius r_{vir} is defined as the radius inside of which the average halo density is Δ_{vir} times the critical density for closure. For the Λ CDM cosmology adopted here $\Delta_{\text{vir}} \simeq 101$ (Bryan & Norman 1998). For the halo concentration parameter we adopt the model of Bullock et al. (2001c):

$$c(M_{\text{vir}}, z) = 4.0 \left(\frac{1+z_{\text{coll}}}{1+z} \right) \quad (4)$$

with z_{coll} the redshift at which a halo with one percent of the present day virial mass collapses.

Finally we consider a distribution of halo spin parameters given by

$$p(\lambda) d\lambda = \frac{1}{\sigma_{\lambda} \sqrt{2\pi}} \exp \left(-\frac{\ln^2(\lambda/\bar{\lambda})}{2\sigma_{\lambda}^2} \right) \frac{d\lambda}{\lambda}, \quad (5)$$

with $\bar{\lambda} = 0.06$ and $\sigma_{\lambda} = 0.6$. This log-normal distribution accurately fits the distribution of λ for haloes in N -body simulations (e.g., Barnes & Efstathiou 1987; Ryden 1988; Cole & Lacey 1996; Warren et al. 1992).

2.2 The formation of disc and bulge

In order to compute the formation and evolution of the discs we proceed as follows. Each time step Δt a new mass shell virializes. The mass and angular momentum of that shell are computed from the MAH and the requirement that the spin parameter remains constant, respectively. A fraction $f_{\text{bar}} = \Omega_{\text{bar}}/\Omega_0$ of this mass is in baryons, and is heated to the halo’s virial temperature. The baryons dissipate energy radiatively, but are assumed to conserve their specific angular momentum. The time scale on which they reach centrifugal equilibrium in the disc is given by $t_c \equiv \max[t_{\text{ff}}, t_{\text{cool}}]$, with t_{ff} and t_{cool} the free-fall and cooling times, respectively (see paper 1 for the details). We use the collisional ionization equilibrium cooling functions of Sutherland & Dopita (1993), assuming a Helium mass abundance of 0.25. The metallicity of the hot gas, Z_{hot} , is considered a free model parameter.

Self-gravitating discs tend to be unstable against global instabilities such as bar formation. Here we follow the approach of van den Bosch (1998, 2000) and Avila-Reese & Firmani (2000) and assume that an unstable disc transforms part of its disc material into a bulge component in a self-regulating fashion such that the final disc is marginally stable. We consider the disc to be unstable if

$$\alpha_{\text{max}} = \max_{0 \leq r \leq r_{\text{vir}}} \left(\frac{V_{\text{disc}}(r)}{V_{\text{circ}}(r)} \right) < 0.7. \quad (6)$$

(Christodoulou, Shlosman & Tohline 1995). Here $V_{\text{disc}}(r)$ and $V_{\text{circ}}(r)$ are the circular velocities of the disc (cold gas plus stars) and the composite disc-bulge-halo system, respectively. Throughout we assume that the disc is infinitesimally thin, and each time step we use the adiabatic invariant formalism of Blumenthal et al. (1986) and Flores et al. (1993) to compute the gravitational contraction of the dark matter induced by the baryons settling in the disc.

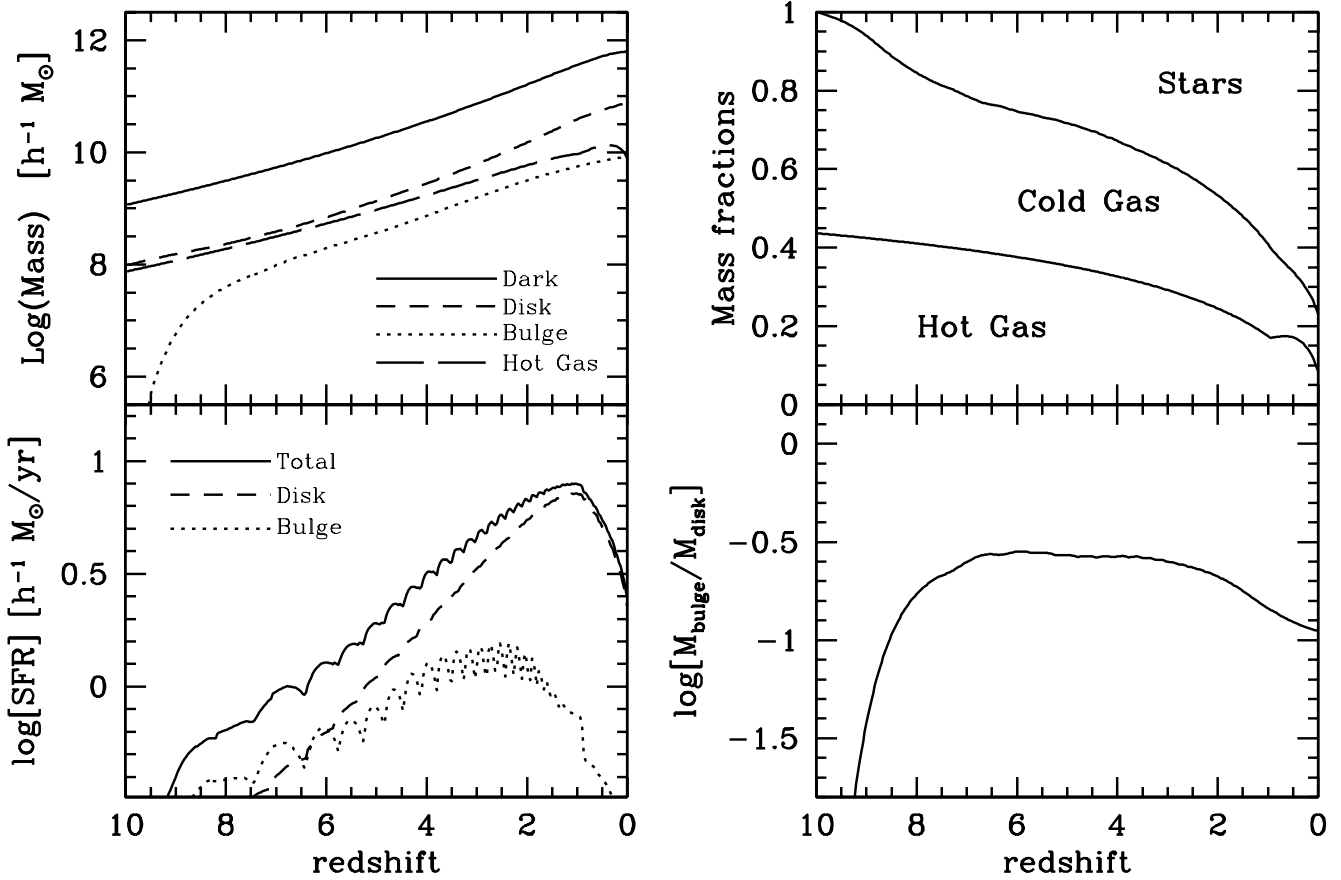


Figure 2. Some results for our fiducial model galaxy discussed in Section 3. The upper left panel plots the mass evolution of various components, as indicated. In the upper panel on the right, the cumulative baryonic mass fractions are plotted, which show how initially all the baryons are in the gas phase (either hot or cold), which is rapidly converted into stars. The star formation histories of the disc and bulge are plotted in the lower left panel, while the lower right panel shows how the bulge-to-disc mass ratio evolves with time.

2.3 Star formation and Feedback

For the star formation rate we adopt the standard Schmidt (1959) law:

$$\psi(R) = 2.5 \times 10^{-4} \text{ M}_{\odot} \text{ yr}^{-1} \text{ kpc}^{-2} \left(\frac{\Sigma_{\text{gas}}(R)}{1.0 \text{ M}_{\odot} \text{ pc}^{-2}} \right)^{1.4} \quad (7)$$

where the numerical values are determined observationally (Kennicutt 1998). This simple empirical law holds over many orders of magnitude in gas surface density, and even applies to circum-nuclear starburst regions. However, when applied to *local* gas densities, the Schmidt law breaks down at large disc radii, where the star formation is found to be abruptly suppressed. In a seminal paper, Kennicutt (1989) showed that these radii correspond to the radii where the gas surface density falls below the critical surface density given by Toomre's (1964) stability criterion:

$$\Sigma_{\text{crit}}(R) = \frac{\sigma_{\text{gas}} \kappa(R)}{3.36 G Q}. \quad (8)$$

Here Q is a dimensionless constant near unity, σ_{gas} is the velocity dispersion of the gas, and κ is the epicycle frequency. Each time step, and for each radial bin, we compute the mass in cold gas that is transformed into stars by solving $d\Sigma_{\text{gas}}/dt = -\psi$ with the constraint that Σ_{gas} can not be depleted below Σ_{crit} . Throughout we adopt $Q = 1.5$ and

$\sigma_{\text{gas}} = 6 \text{ km s}^{-1}$ (Kennicutt 1989). The gas that is transferred into the bulge component is assumed to form stars instantaneously with 100 percent efficiency.

In addition to the simple Schmidt law, we have also experimented with a star formation rate given by

$$\psi(R) = 0.017 \Sigma_{\text{gas}}(R) \frac{V_c(R)}{R} \quad (9)$$

(Silk 1997), again combined with the star formation threshold criterion. With this parameterization each orbit ~ 10 percent of the available cold gas is transformed into stars. As shown by Kennicutt (1989), this description yields an equally good fit to the data as the Schmidt-law of equation (7). As it turns out, our models yield virtually indistinguishable results for both SFRs, and we therefore adhere to the Schmidt-law description in what follows.

When stars evolve they put energy into the interstellar medium (ISM) which impacts on the further evolution of the galaxy. By resorting to an empirical description of the star formation, we are implicitly taking account of the effects that these feedback processes have on the star formation rate. What is not taken into account, however, is a possible feedback-driven outflow of gas from the disc. Here we use a simple parametric model, similar to the ones used in various semi-analytical models for galaxy formation. We assume that the amount of gas blown out of the disc is proportional

to the total energy input by supernovae (SNe) and inversely proportional to the escape velocity squared. At each radial bin, the cold gas mass that is ejected is given by

$$\Delta M_{\text{eject}} = \frac{\varepsilon_{\text{fb}} \eta_{\text{SN}} E_{\text{SN}}}{V_{\text{esc}}^2} \Delta M_* \quad (10)$$

(cf. Kauffmann et al. 1993; Natarajan 1999). Here $E_{\text{SN}} = 10^{51}$ ergs is the energy produced by one SN, η_{SN} is the number of SNe per solar mass of stars formed, V_{esc} is the local escape velocity, and ε_{fb} is a free parameter that describes what fraction of the energy released by SNe is converted into kinetic energy to drive the outflow. For simplicity, we assume that the ejected mass is forever lost from the system: the ejected mass is not considered for later infall, and the corresponding metals are not used to enrich the infalling gas.

2.4 Stellar population modeling & chemical evolution

In order to convert the stellar masses into luminosities we use the latest version of the Bruzual & Charlot (1993) stellar population synthesis models. These models provide the luminosities of a single burst stellar population as function of age t and metallicity Z in various optical passbands. In order to model the chemical enrichment of the ISM we follow the standard instantaneous recycling approximation (IRA). We assume that a fraction \mathcal{R} of the mass in stars formed is instantaneously returned to the cold gas phase with a yield y (which is defined as the fraction of mass converted into stars that is returned to the ISM in the form of newly produced metals).

In each disc annulus, and at each time step, mass conservation implies

$$\Delta M_{\text{cold}} = \Delta M_{\text{cool}} - (1 - \mathcal{R})\Delta M_* - \Delta M_{\text{eject}} \quad (11)$$

and for the mass in metals one thus obtains

$$\begin{aligned} \Delta M_{\text{metal}} = & Z_{\text{hot}}\Delta M_{\text{cool}} - Z_{\text{cold}}\Delta M_{\text{eject}} - \\ & Z_{\text{cold}}(1 - \mathcal{R})\Delta M_* + y\Delta M_* \end{aligned} \quad (12)$$

Here ΔM_{cool} is the mass that, in the given time step, has cooled, and ΔM_* is the mass that is transformed into stars. We use these two equations to track the evolution of the metallicity of the cold gas in the disc, Z_{cold} , as function of both time and radius. Throughout we adopt the Scalo (1986) IMF, for which $\eta_{\text{SN}} = 4 \times 10^{-3} \text{ M}_{\odot}^{-1}$ and $\mathcal{R} = 0.25$. The stellar yield y , finally, is left a free parameter.

2.5 Missing Ingredients

It is important to understand the various shortcomings of the models discussed above. First of all, for each galaxy we adopt the *average* mass accretion history for systems of that mass. In reality there is a relatively large scatter in MAHs (see Figure 1), which introduces some additional scatter in for instance the star formation rates, and thus the colors of our model galaxies (cf. right panels of Figure 3). Furthermore, in our models all halos of a given mass have the same concentration parameter, whereas in reality dark matter halos reveal a relatively large amount of scatter in $c(M_{\text{vir}})$ (Jing 2000; Bullock et al. 2001c). In fact, Wechsler

et al. (2001) have shown that the halo concentration parameter is strongly correlated with the MAH. None of these effects are taken into account here. Also, by assuming that all mass is accreted in a smooth fashion we ignore the effect of discrete mergers. Although the fragility of disks (Tóth & Ostriker 1992) suggests that mergers can not have played a dominant role during their formation, some amount of merging almost certainly occurs. Since we ignore all these effects, each model galaxy should be regarded as averaged over all its possible MAHs, which underestimates the amount of scatter in various properties of our model galaxies. However, we are not attempting to compare our models to data. Instead our main goal is to investigate the impact that cooling and feedback have on the models, and underestimating the scatter will only help to highlight these effects.

An important oversimplification of our models is the treatment of the galactic winds. We assume that any material expelled by supernova feedback escapes the halo without enriching the hot halo gas. In reality some of the outflowing material may remain bound to the halo, enrich the hot gas (which increases its cooling efficiency), and later cool back onto the disc. However, very little is known about how the outflowing, enriched material interacts with the hot halo gas. Therefore, rather than introducing some additional free parameters to our models, we have simply chosen a (perhaps somewhat extreme) prescription. As emphasized above, our main goal is to investigate how we may hope to infer $f_{\text{gal}}(M_{\text{vir}})$ from observations. For this purpose, the models do not necessarily have to yield the most physical/accurate estimate of the true $f_{\text{gal}}(M_{\text{vir}})$.

3 A FIDUCIAL MODEL GALAXY

Before we investigate large samples of model disc galaxies, it is useful to investigate one particular model galaxy in more detail. We exclude feedback for the moment (i.e., $\varepsilon_{\text{fb}} = 0$) and assume that baryons that enter the virial radius have already been enriched to one-third Solar metallicity ($Z_{\text{hot}} = Z_{\odot}/3$). A particular model galaxy is parameterized by its present day virial mass $M_{\text{vir}}(0)$ and its spin parameter λ . We focus on a model galaxy with $M_{\text{vir}}(0) = 5 \times 10^{11} h^{-1} \text{ M}_{\odot}$ and $\lambda = 0.06$. The MAH is given by the Universal form of equation (1). These parameters result in a model galaxy that is fairly similar to the Milky Way (MW): at $z = 0$ the model galaxy has a disc scale length of 4.5 kpc, a rotation velocity at 8.5 kpc of 230 km s^{-1} , and a bulge-to-disc mass ratio of 0.1. We tune the yield to $y = 0.01$ so that the cold gas at 8.5 kpc from the center has solar metallicity.

The upper left panel of Figure 2 plots the evolution of the various mass components with time (redshift). The upper panel on the right plots the cumulative mass fractions of the baryons inside the virial radius that at each redshift are in the form of hot gas, cold gas (in the disc), and stars (in both the disc and bulge). At $z = 10$, when we start our model computations, about 50 percent of the baryonic mass inside the virial radius is in the hot gas phase, while the rest has already had time to cool. Star formation immediately sets in, transferring more and more of the cold gas into stars, while at the same time new baryons enter the virial radius, are heated to the virial temperature, and cool to become part of the cold gas in the disc. At $z = 0$

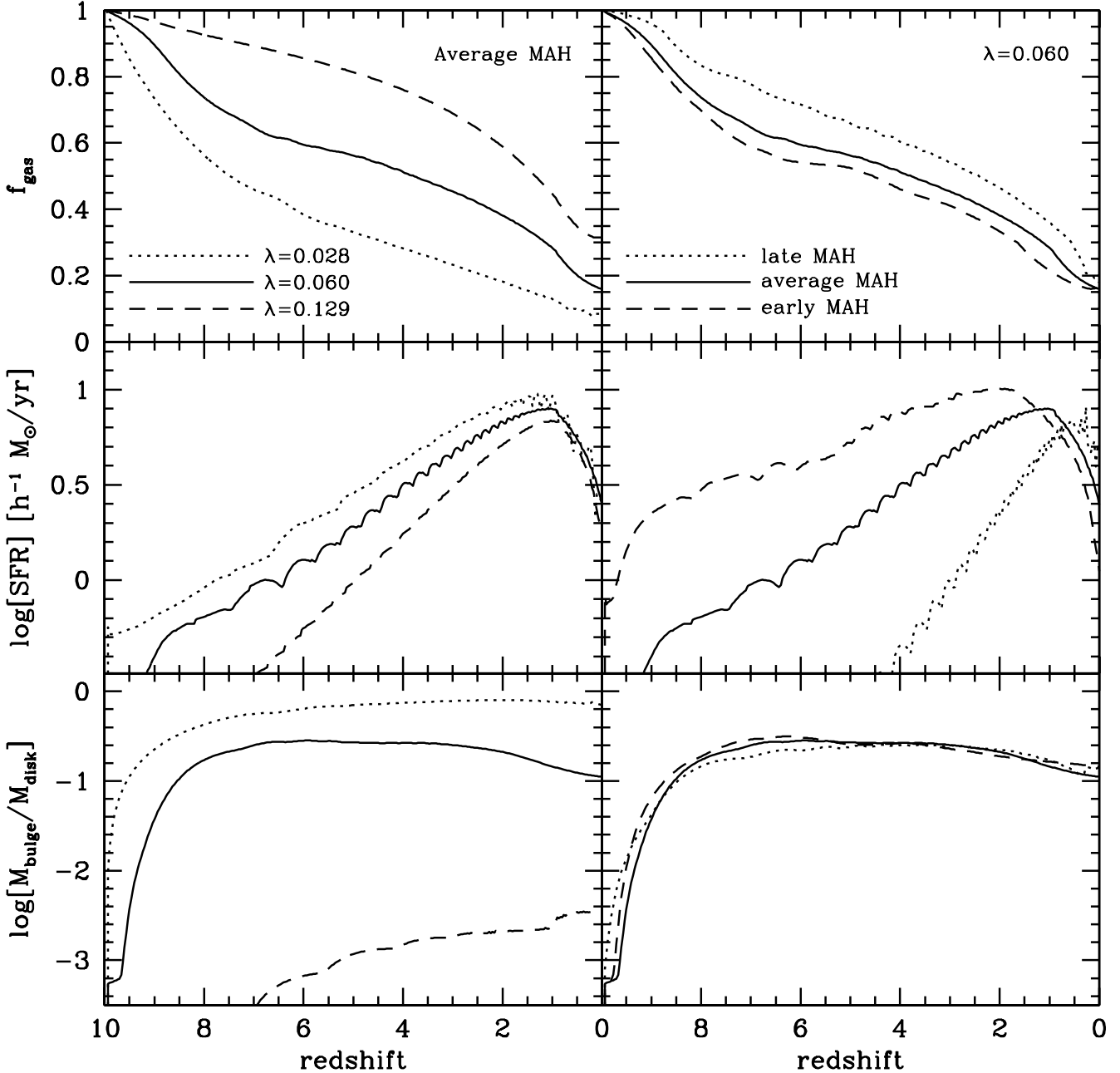


Figure 3. The influence of changes in spin parameter (left panels) and MAH (right panels) on the outcome of our fiducial model galaxy. From the top to bottom we plot the disc gas mass fractions, the total (disc plus bulge) star formation rates, and the bulge-to-disc mass ratios, all as functions of redshift. Haloes with less angular momentum produce more bulge-dominated disc galaxies with lower gas mass fractions. The MAH mainly sets the star formation history of the galaxies, but does not significantly influence the structural parameters.

about 80 percent of all the baryonic mass is in the form of stars, while the remaining 20 percent is roughly equally split amongst cold and hot gas. The lower right panel plots the bulge-to-disc mass ratio (B/D) as function of time. At $z \simeq 9$ the disc becomes unstable and a bulge starts to form, rapidly increasing B/D to about 0.3. At later times ($z \lesssim 2$) the bulge-to-disc ratio slowly decreases again to a present day value of ~ 0.1 . Finally, the lower left panel of Figure 2 plots the star formation rates (SFRs) of both the disc and bulge. At high redshifts ($z \gtrsim 5$) the disc and bulge have very comparable SFRs. At lower redshifts the disc clearly dom-

inates the total SFR, which peaks at $z \sim 1$, after which is declines rapidly to a present day SFR of $\sim 3 \text{ M}_{\odot} \text{ yr}^{-1}$. The ‘wobbly’ behavior of the SFR of the bulge is an artifact of the way bulge formation is taken into account in the models, but does not influence any of our results.

3.1 Model dependence on spin parameter and mass accretion history

In order to gauge the dependence of the model galaxies on the halo spin parameter we compare model galaxies with

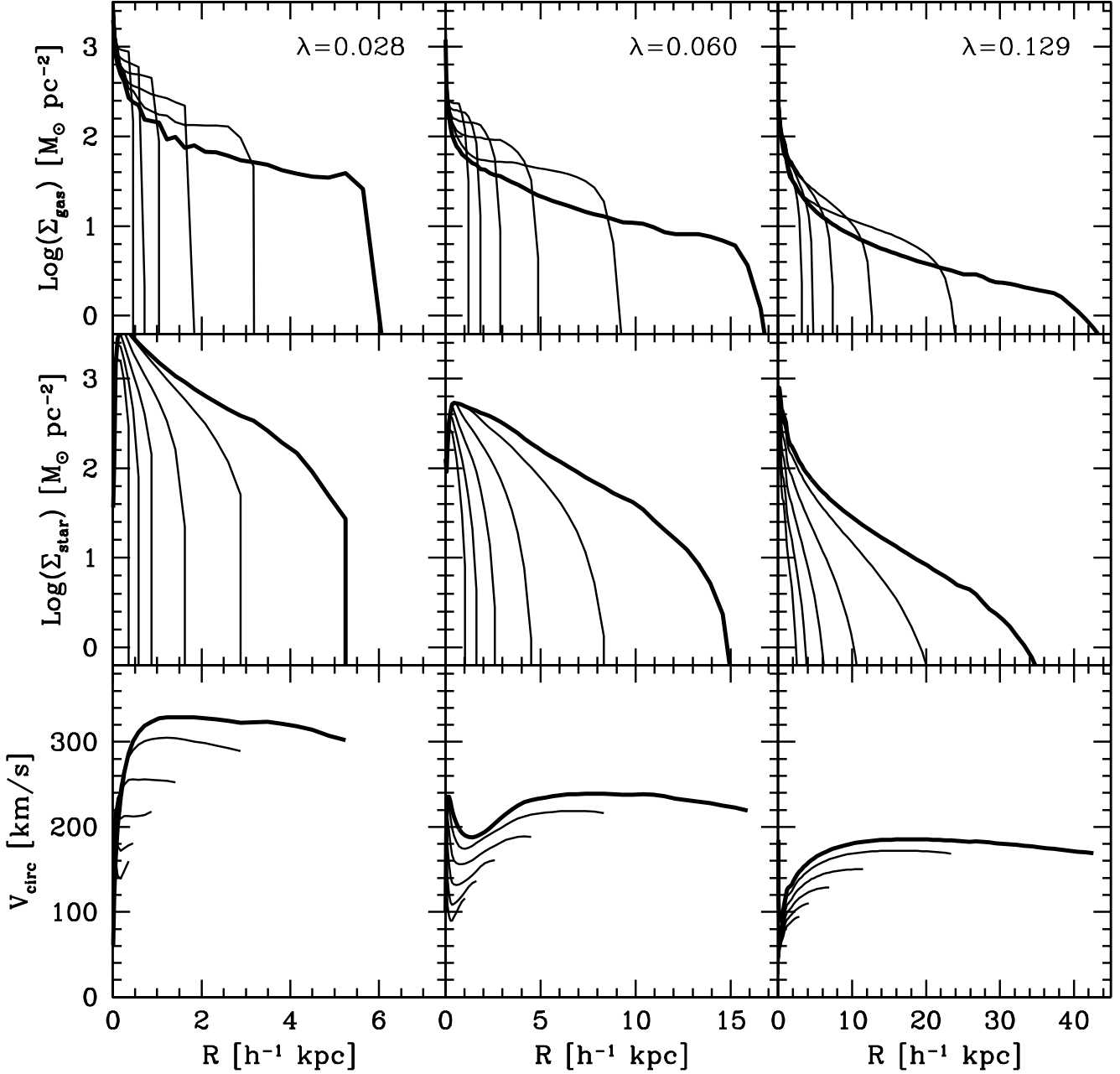


Figure 4. The evolution of the surface densities of cold gas (top panels), stars (middle panels), and rotation curves (bottom panels), all as function of galactocentric radius, for three models with $M_{\text{vir}} = 5 \times 10^{11} h^{-1} M_{\odot}$ and different halo spin parameters (as indicated in the top panels). The thick lines correspond to the present day ($z = 0$), while the various thin lines correspond to $z = 5, 4, 3, 2, 1$. Note the inside-out character of the disc formation, the close to exponential surface density distributions of the stars, and the flat rotation curves.

$\lambda = 0.028, 0.06$, and 0.129 . These values correspond to the 10, 50, and 90 percentile points of the distribution of equation (5) with $\bar{\lambda} = 0.06$ and $\sigma_{\lambda} = 0.6$. In addition to mass and angular momentum, the actual mass accretion history of a dark matter halo can also impact on the final outcome of the model galaxy. Although for the remainder of this paper we adopt the universal MAH of equation (1), which corresponds to the *average* of a large ensemble of possible MAHs, it is important to understand how the models depend on variations of the MAH with respect to the average. To that extent we construct three models (with $M_{\text{vir}}(0) = 5 \times 10^{11} h^{-1} M_{\odot}$ and

$\lambda = 0.06$) that only differ in their MAHs. These MAHs are plotted in Figure 1: in addition to the average MAH (thick solid line) we consider an early (dashed line) and a late (dotted line) MAH, which roughly outline the distribution of possible MAHs for a halo with $M_{\text{vir}}(0) = 5 \times 10^{11} h^{-1} M_{\odot}$.

In Figure 3 we show the effects that a change in spin parameter (left panels) and MAH (right panels) have on the outcome of the fiducial model presented in Figure 2. The halo spin parameter determines mainly the bulge-to-disc ratio: the high- λ model is virtually bulgeless and with a disc gas mass fraction f_{gas} about twice as high as for the $\lambda =$

0.06 model. Here $f_{\text{gas}} = M_{\text{cold}}/(M_{\text{cold}} + M_{\text{star}})$ with M_{cold} and M_{star} the disc masses in cold gas and stars, respectively. The low angular momentum halo with $\lambda = 0.028$ results in a galaxy for which the bulge mass is almost equal to that of the disc (i.e., the resulting galaxy is more reminiscent of an S0 than a spiral galaxy). Although the spin parameter has a mild influence on the SFR at $z \gtrsim 1$, the present day SFR is virtually independent of λ : although systems with a lower value of λ have a higher surface density, and therefore a higher star formation rate *per unit area*, they are also smaller, such that the total, area-integrated star formation rate depends only weakly on λ . The MAH, on the other hand, strongly influences the SFR, even at $z = 0$, suggesting that the rate at which stars form is directly linked to the rate at which the galaxy accretes mass. The disc gas mass fraction and bulge-to-disc ratio do not depend strongly on the MAH, especially not at $z = 0$. Note that in our models bulges form only as a consequence of disk instabilities. In reality, part of the bulge may also form out of mergers of sub-clumps, in which case the bulge-to-disk ratio may depend more strongly on the MAH than is the case here.

In Figure 4 we plot the surface densities of the cold gas (upper row) and disc stars (middle row) as functions of galactocentric radius at six different redshifts: $z = 5, 4, 3, 2, 1, 0$ with the latter one plotted as thick solid lines. Results are plotted for three different values of the halo spin parameter as indicated in the top panels. All these models have $M_{\text{vir}}(0) = 5 \times 10^{11} h^{-1} M_{\odot}$ and an average MAH. The evolution of the disc surface densities with redshift clearly illustrates the inside-out growth of the disc; already at high redshift the central surface densities of the stellar discs are established, while at $z = 1$ the disc is still only about half the present day size. At each redshift the stellar disc nicely follows an exponential profile with a distinct outer truncation radius[†]. The surface density distribution of the cold gas is much shallower than that of the stars, in good agreement with observations. See paper 1 for a more detailed discussion of why the gas and cold gas follow distinct surface density distributions.

The lower panels of Figure 4 plot the circular velocity curves of the model galaxies (plotted out to the maximum radius at which cold gas is available, to mimic what an observer might be able to measure) at the same redshifts. The present day rotation curve of the $\lambda = 0.06$ model (middle column) peaks at small radii, reflecting the presence of the bulge, reaches a minimum of $\sim 200 \text{ km s}^{-1}$ at about 2 kpc, and becomes fairly flat at larger radii with $V_{\text{circ}} \sim 230 \text{ km s}^{-1}$. All these features are in remarkably good agreement with the MW rotation curve (Burton & Gordon 1978). The rotation curves for the other two models are more featureless, lacking any obvious transition region from either the bulge- or halo-dominated region to the disc-dominated region. The lack of such a feature, often referred to as the ‘disc-halo’ conspiracy (e.g., van Albada et al. 1985) is in good agreement with data, which shows that there is nothing conspicuous about it.

[†] An exception is the $z = 0$ stellar surface density profile of the $\lambda = 0.129$ model, which is more centrally concentrated than an exponential. This indicates a problem for the models which is discussed in detail in Paper 1

Table 1. Overview of Model Parameters.

| Model | Z_{hot}/Z_{\odot} | ε_{fb} | y |
|---------|----------------------------|---------------------------|-------|
| PE-NFB | 0.3 | 0.0 | 0.010 |
| NPE-NFB | 0.0 | 0.0 | 0.015 |
| PE-LFB | 0.3 | 0.02 | 0.015 |
| PE-MFB | 0.3 | 0.05 | 0.025 |
| PE-HFB | 0.3 | 0.10 | 0.040 |
| NPE-LFB | 0.0 | 0.02 | 0.024 |

Column (1) lists the model ID. Columns (2) – (4) give the metallicity of the hot gas (in units of solar metallicity), the feedback efficiency, and the stellar yield, respectively.

4 THE BARYONIC MASS FRACTIONS OF DISC GALAXIES

In this paper we consider six models that only differ in the metallicity of the hot gas, Z_{hot} , the feedback efficiency, ε_{fb} , and the stellar yield y . The parameters used are listed in Table 1. All other model parameters are kept fixed at their fiducial values (see Section 2). Our prime focus in this paper will be a comparison between the first three models. The PreEnrichment No Feedback model (PE-NFB) with $Z_{\text{hot}} = 0.3Z_{\odot}$, a typical value for the hot gas in clusters (Mushotzsky & Loewenstein 1997), and $\varepsilon_{\text{fb}} = 0$, the No PreEnrichment No Feedback model (NPE-NFB) with $Z_{\text{hot}} = 0.0$ and $\varepsilon_{\text{fb}} = 0$, and the PreEnrichment Low-FeedBack model (PE-LFB) with $Z_{\text{hot}} = 0.3Z_{\odot}$ and $\varepsilon_{\text{fb}} = 0.02$ (i.e., two percent of the SN energy is converted to kinetic energy). In each model the yield is tuned so that the cold gas in the fiducial MW-like model discussed in Section 3 has solar metallicity at the solar radius. For each model we construct samples of 400 model galaxies. Present day virial masses are drawn from the Press-Schechter (1974) mass function with $10^{10} h^{-1} M_{\odot} \leq M_{\text{vir}}(0) \leq 10^{13} h^{-1} M_{\odot}$. This corresponds to haloes with circular velocities in the range $31 \text{ km s}^{-1} \leq V_{\text{vir}} \leq 312 \text{ km s}^{-1}$, roughly the range expected for galaxies. Spin parameters are drawn from the log-normal distribution of equation (5), and for each model galaxy we use the Universal MAH of equation (1). We are mainly interested in spiral galaxies (of type Sa and later). Therefore, galaxies that are too bulge-dominated are removed from the sample. Following Simien & de Vaucouleurs (1986) we use the criterion that the total galaxy has to be at least 0.98 magnitudes brighter than the bulge in the B -band.

4.1 Theoretical Predictions

In the upper panels of Figure 5 we plot the present day galaxy mass fractions $f_{\text{gal}} = M_{\text{gal}}/M_{\text{vir}}$ as function of M_{vir} (for models PE-NFB, NPE-NFB, and PE-LFB only). Here M_{gal} is defined as the mass of the galaxy (disc + bulge), which includes all the baryons inside the virial radius minus the hot halo gas and the gas that is expelled from the disc in SN-driven outflows. In the PE-NFB Model (left panels) f_{gal} is virtually identical to the universal baryon fraction f_{bar} (indicated by the horizontal dotted line) for systems with $M_{\text{vir}}(0) \lesssim 5 \times 10^{11} h^{-1} M_{\odot}$. For more massive systems the cooling is less efficient and f_{gal} decreases strongly with increasing virial mass. This is even more pronounced in model NPE-NFB (middle panels) where cooling is less efficient and f_{gal} already drops below f_{bar} at $M_{\text{vir}} \sim 5 \times 10^{10} h^{-1} M_{\odot}$. For zero-metallicity gas the cooling time is so long that for

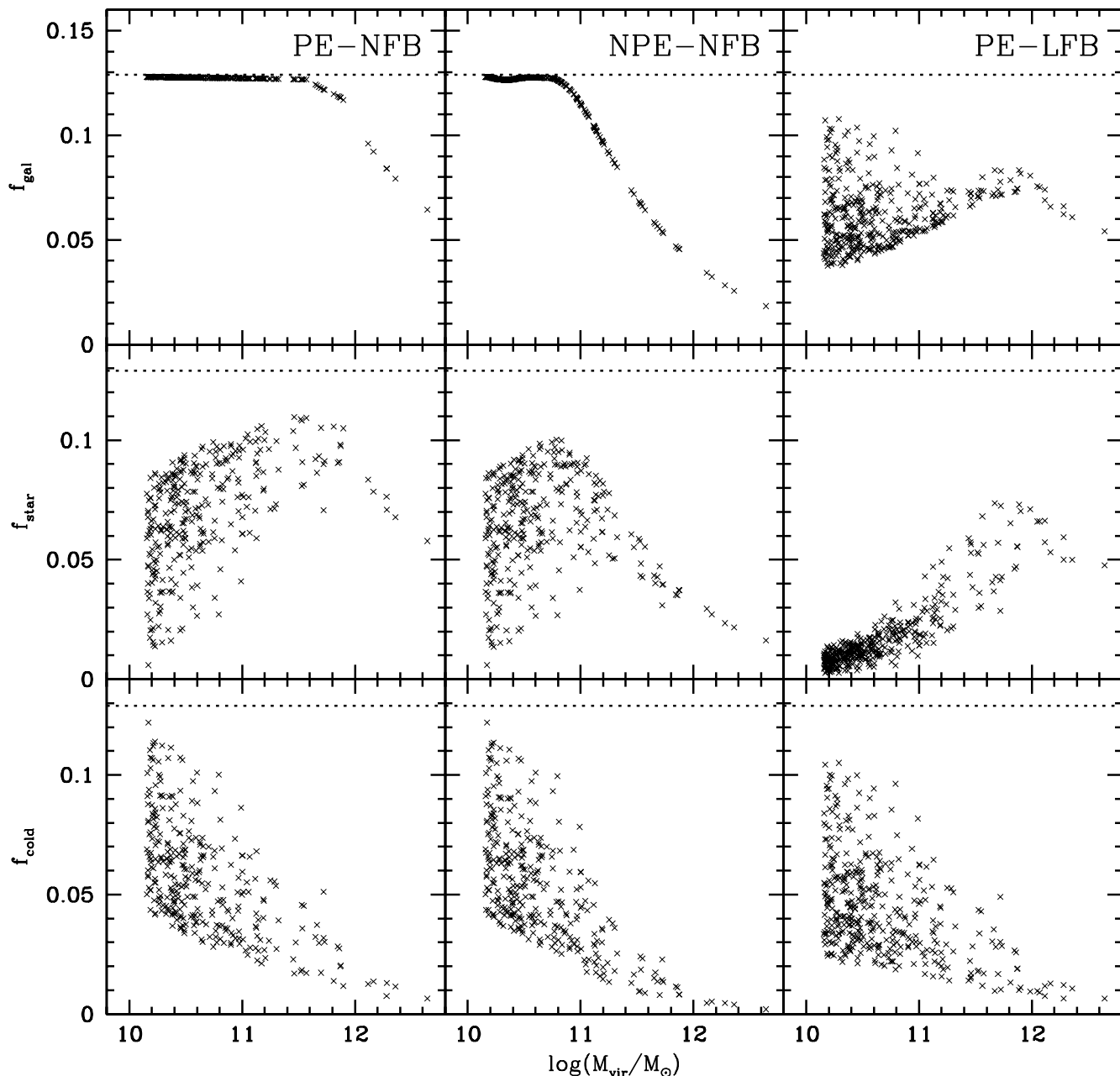


Figure 5. Upper panels plot the present day galaxy mass fractions f_{gal} as function of virial mass for samples of three different models: the PreEnrichment model with No FeedBack (PE-NFB, left), the No PreEnrichment, No FeedBack model (NPE-NFB, middle), and the PreEnrichment Low-FeedBack Model (PE-LFB, right). These models only differ in the feedback efficiency, the metallicity of the hot gas, and the stellar yield, as indicated in Table 1. The lower two rows of panels show how the galaxy mass is split up in stars (f_{star}) and cold gas (f_{cold}). The dotted lines correspond to the universal baryon fraction f_{bar} which indicates the maximum possible value of f_{gal} . In the two models without feedback (PE-NFB and NPE-NFB), f_{gal} depends only on the fraction of baryons that can cool and is therefore independent of λ . When feedback is included (as in Model PE-LFB), f_{gal} also depends on the halo spin parameter, resulting in a large amount of scatter at the low mass end (where feedback is most effective). Note also that feedback impacts mainly on f_{star} , not on f_{cold} .

massive galaxies with $M_{\text{vir}}(0) \simeq 10^{13} h^{-1} M_{\odot}$ only about 15 percent of all the baryons inside the virial radius have had sufficient time to cool. In model PE-LFB (right panels), $f_{\text{gal}} \ll f_{\text{bar}}$ for the low mass systems, but with a large amount of scatter. This is a reflection of the scatter in halo spin parameters: systems with less angular momentum produce discs with higher surface densities, therefore have higher star formation rates, which induce a more ef-

ficient feedback. At the high mass end f_{gal} is fairly similar to the PE-NFB model without feedback. This owes to the fact that the mass ejection efficiency scales inversely with the square of the escape velocity (see equation [10]), making feedback less efficient in more massive systems.

The panels in the middle and lower rows plot the mass fractions of stars (disc plus bulge), f_{star} , and cold gas, f_{cold} . Note how f_{cold} depends only weakly on both Z_{hot} and ε_{fb} :

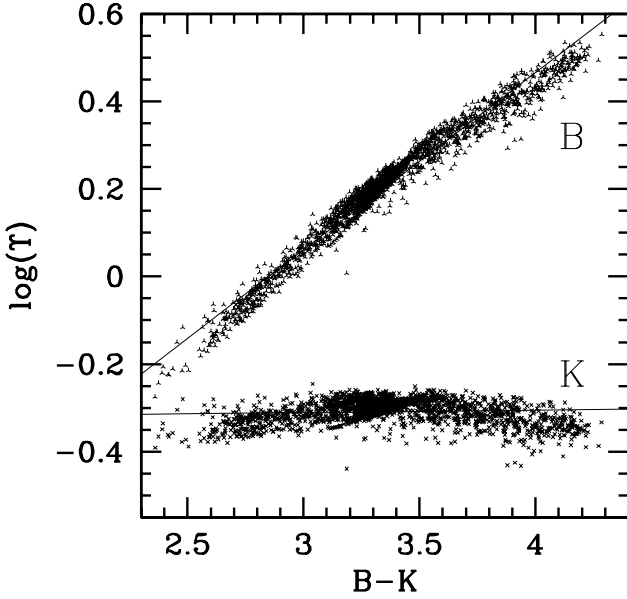


Figure 6. The logarithm of the stellar mass-to-light ratios in the B (tripods) and K (crosses) bands as functions of the $B - K$ color for all galaxies in all six models listed in Table 1. Note the narrow, almost linear, relation, which is fitted by the solid lines (equations [13] and [14]). This indicates that photometric color can be used as an accurate indicator of the stellar mass-to-light ratio (see also Bell & de Jong 2001).

changes in the cooling and feedback efficiencies mainly influence the stellar mass fractions, not the gas mass fractions.

As shown above $f_{\text{gal}}(M_{\text{vir}})$ depends strongly on both the cooling and feedback efficiencies. Therefore, if one could obtain a measure of $f_{\text{gal}}(M_{\text{vir}})$ observationally it would allow us to constrain the poorly understood physics of cooling and feedback. This requires one to be able to infer both the baryonic galaxy mass M_{gal} as well as the total virial mass M_{vir} from observations of the luminous (and gaseous) components. We now use our models to investigate which observables are best suited as the appropriate mass indicators.

4.2 Determining the baryonic mass of disc galaxies

For the total baryonic galaxy mass one can write $M_{\text{gal}} = \Upsilon_k L_k + M_{\text{gas}}$. Here L_k is the luminosity in photometric pass-band k , Υ_k is the corresponding stellar mass-to-light ratio, and M_{gas} is the total gaseous mass of the galaxy. Note that it is apparent from the lower two panels of Figure 5 that one can not ignore the gas mass, which can easily exceed the total stellar mass, especially in low-mass systems. However, measuring M_{gas} is complicated by the fact that the gas component of (disc) galaxies is a multi-phase component, consisting of atomic, molecular, and warm gas. Since our models do not consider such a multi-phase medium, we can not make useful predictions for the accuracy with which one can hope to measure M_{gas} . Therefore, we simply assume for the moment that M_{gas} can be obtained accurately from HI observations (with the appropriate scaling to take account

of Helium), and we warn the reader that we are thus underestimating the uncertainties related to determining M_{gal} .

An important source of error in determining M_{gal} is the unknown stellar mass-to-light ratio Υ . However, in a recent paper Bell & de Jong (2001), have shown that Υ is strongly correlated with color. In particular, they showed that the relation between Υ and color depends only weakly on the star formation history and on dust extinction effects. The main uncertainties are related to the unknown IMF: although the wrong IMF causes a zero-point offset, it conserves the slope of the relation. These results therefore suggest that using multi-color photometry one should be able to obtain fairly accurate estimates of the *relative* stellar mass-to-light ratios of disc galaxies.

In Figure 6 we plot Υ_B and Υ_K , averaged over the entire disc plus bulge, as function of $B - K$ for all galaxies in all six models listed in Table 1. As can be seen, our models, which use the Bruzual & Charlot stellar population models with a Scalo IMF and the IRA for chemical evolution, also reveal a narrow correlation between stellar mass-to-light ratio and $B - K$ color, in excellent agreement with the results of Bell & de Jong. Linear fits (indicated by thin lines) yield

$$\log(\Upsilon_B) = 0.405(B - K) - 1.155 \quad (13)$$

and

$$\log(\Upsilon_K) = 0.005(B - K) - 0.327 \quad (14)$$

We have also computed the colors and mass-to-light ratios of individual radial bins in a given model galaxy, rather than the parameters averaged over the entire model galaxies, and find that these results overlap with those plotted in Figure 6. We therefore conclude that, modulo the uncertainty in the stellar IMF, multi-color photometry of disc galaxies should in principle allow a fairly accurate determination of the total stellar mass of disc galaxies.

4.3 Determining the virial mass of disc galaxies

For virialized systems $M_{\text{vir}} \propto V_{\text{vir}}^3$, with V_{vir} the halo circular velocity at the virial radius. Unfortunately, one cannot measure the circular velocity out at the virial radius. Instead, one can only measure the rotation velocities of the stars and gas in the disc. In the upper panels of Figure 7 we plot V_{max} , defined as the maximum rotation velocity inside the radial extent probed by the cold gas, versus M_{vir} . Results correspond to $z = 0$, and are plotted for all three models. The dotted lines correspond to $V_{\text{max}} \propto M_{\text{vir}}^{1/3}$ and are plotted for comparison (with arbitrary zero-point). Although the average relation between V_{max} and M_{vir} nicely follows this theoretical scaling, in the no-feedback models PE-NFB and NPE-NFB a given value of V_{max} has a corresponding scatter in M_{vir} of a factor six. This large amount of scatter owes entirely to the scatter in λ : the halo angular momentum sets the concentration of the baryonic mass component after cooling, which, together with the effects of adiabatic contraction, causes a large spread in V_{max} at given M_{vir} (cf. the lower panels of Figure 4). Furthermore, although the scatter in model PE-LFB is significantly less, the zero-point of the $M_{\text{vir}}(V_{\text{max}})$ relation is offset with respect to the models without feedback. We thus conclude that V_{max} can not be used as a reliable indicator of the total virial mass.

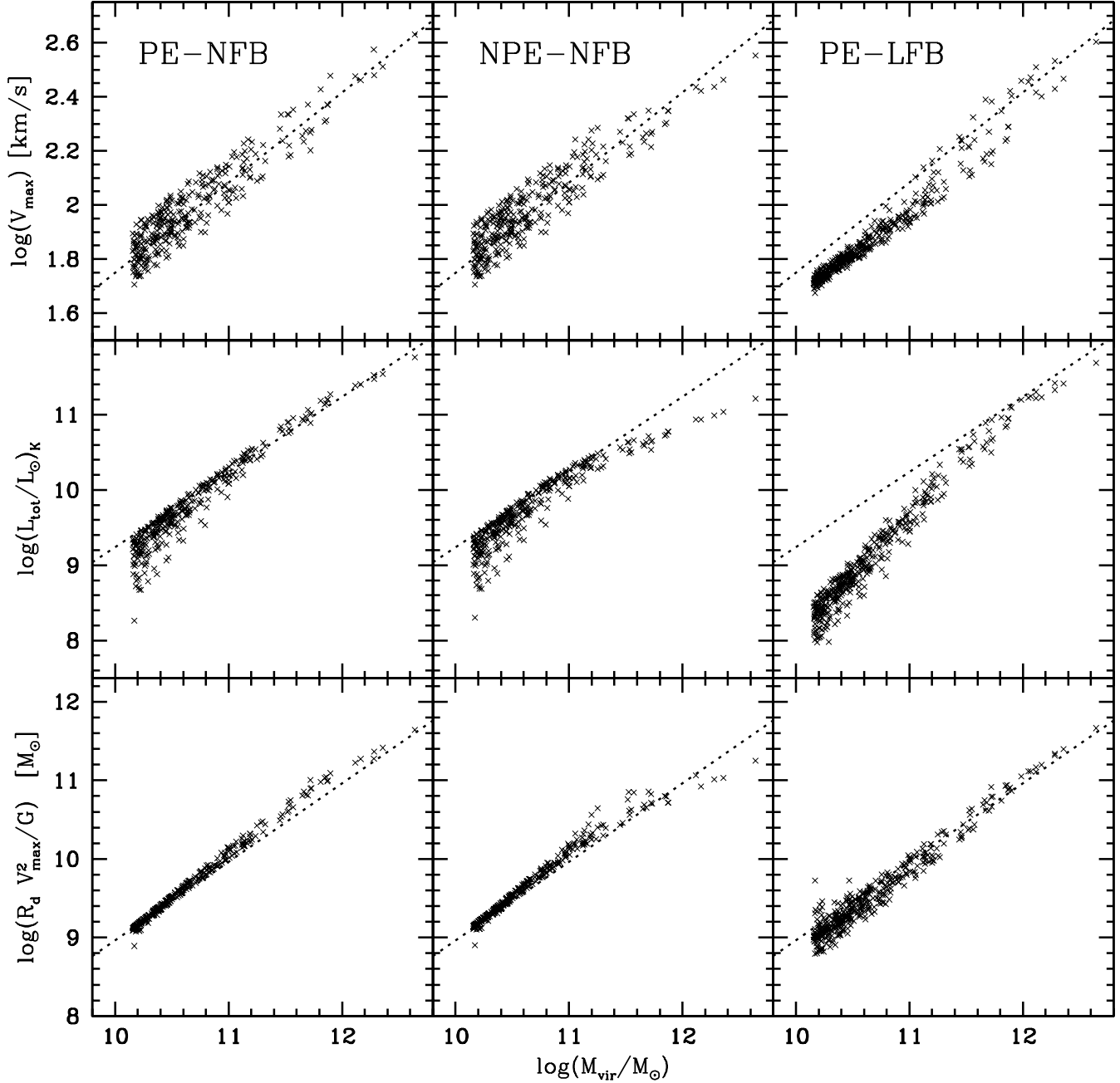


Figure 7. The relation between various virial mass estimators and the actual virial mass for the three models plotted in Figure 5. In the upper panels $\log(V_{\max})$ is plotted versus $\log(M_{\text{vir}})$. The dotted lines correspond to $M_{\text{vir}} \propto V_{\max}^{1/3}$, and is a reasonable description of the average relation. However, the scatter is large, and the zero-point depends on the actual model, which makes V_{\max} unsuitable as virial mass indicator. The same goes for the K -band luminosity, which is plotted in the middle row of panels. Here the dotted lines correspond to $L_K \propto M_{\text{vir}}$, which only yields a reasonable description for the brighter galaxies in models with $Z_{\text{hot}} = Z_{\odot}/3$. For fainter galaxies the scatter is again large. Furthermore the slope of the $L_K(V_{\text{vir}})$ relation depends strongly on the feedback efficiency. In the lower panels we plot the virial mass estimator $R_d V_{\max}^2/G$ as function of M_{vir} . Here the dotted lines correspond to equation (15), which provides a reasonable description of the models, independent of the cooling and/or feedback efficiencies.

Next we investigate how well the total K -band luminosity can be used as indicator of total virial mass (panels in middle row). In model PE-NFB the luminous galaxies nicely follow a relation $L_K \propto M_{\text{vir}}$ with very little scatter. However, for the less luminous systems this narrow relation breaks down. This is a reflection of the fact that less massive systems have a much larger spread in gas mass fractions (cf.

lower panels of Figure 5). In model NPE-NFB one can see a clear curvature at the high-luminosity end, reflecting the cooling inefficiencies. In model PE-LFB there is no longer a linear relation between L_K and M_{vir} due to the higher feedback efficiencies in lower mass systems. Based on these results we thus conclude that total luminosity is also a poor indicator of total virial mass.

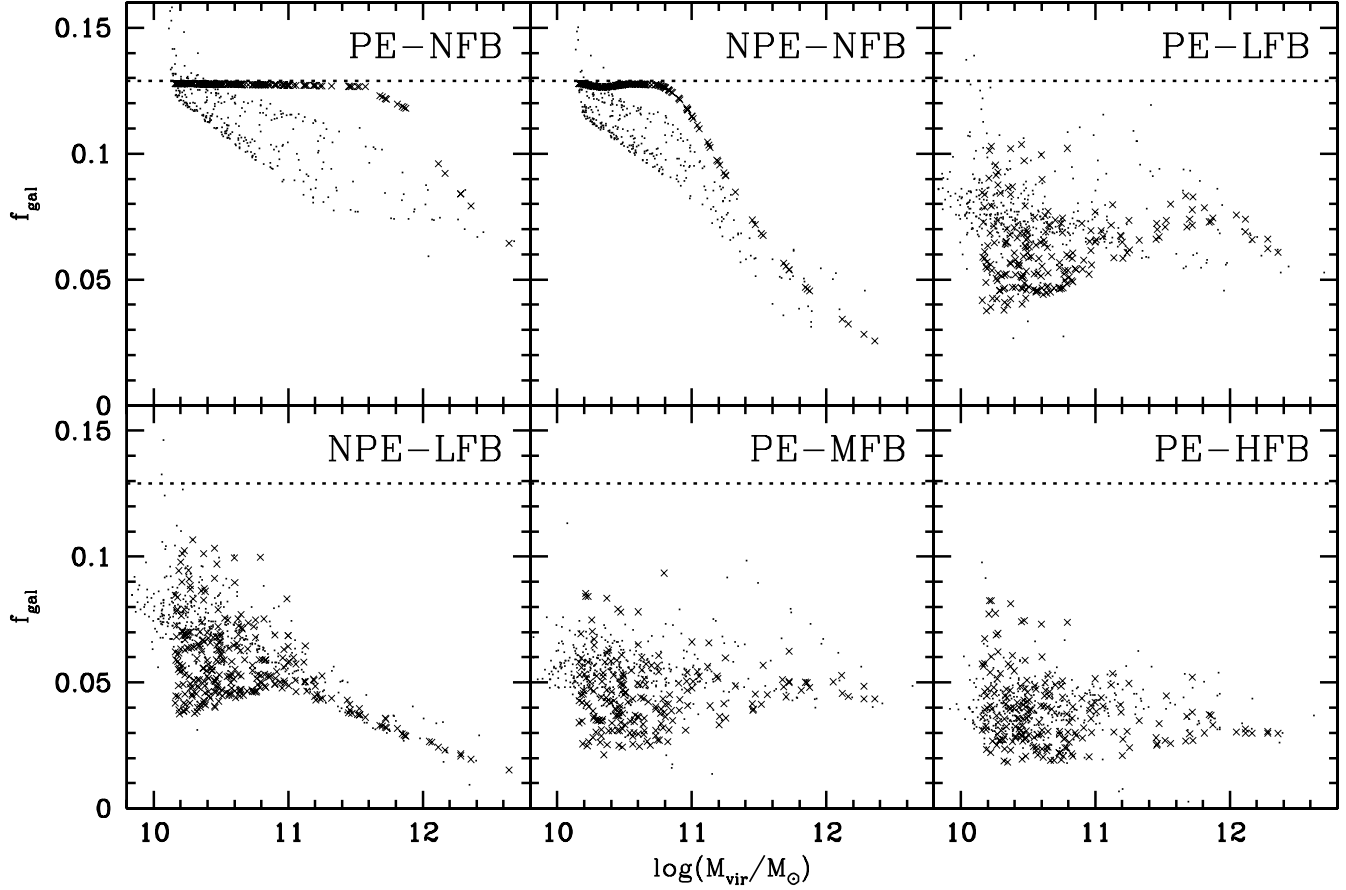


Figure 8. A comparison of the true galaxy mass fraction f_{gal} as function of the true virial mass (crosses) with the same values estimated from the observables extracted from the models (dots). Results are plotted for all six models discussed in this paper. Dotted lines correspond to the universal baryonic mass fraction f_{bar} . In the models with feedback (PE-LFB, NPE-LFB, PE-MFB, and PE-HFB) the dots occupy the same parameter space as the crosses, indicating that the observables allow one to recover $f_{\text{gal}}(M_{\text{vir}})$, at least in a statistical sense. In the two models without feedback (PE-NFB and NPE-NFB) the scatter in the recovered $f_{\text{gal}}(M_{\text{vir}})$ is much larger than in the intrinsic $f_{\text{gal}}(M_{\text{vir}})$, but the former still allows to discriminate between the two models; in particular, the estimated galaxy mass fractions nicely avoid the upper right regions of parameter space which contain information on the cooling efficiencies.

Finally, in the lower row of panels in Figure 7 we plot the mass measure $R_d V_{\text{max}}^2 / G$ versus M_{vir} . Here R_d is the disc scale length in the I -band, obtained from fitting an exponential to the I -band surface brightness distribution of the disc. The dotted lines correspond to the fitting relation

$$M_{\text{vir}} = 2.54 \times 10^{10} M_{\odot} \left(\frac{R_d}{\text{kpc}} \right) \left(\frac{V_{\text{max}}}{100 \text{ km s}^{-1}} \right)^2. \quad (15)$$

The zero-point of this relation is determined by fitting to all model galaxies of all six models simultaneously, and is not necessarily the best fit for one particular model. The model galaxies nicely follow this relation, with an rms scatter between 20 and 50 percent (depending on the amount of feedback). The fraction of model galaxies for which equation (15) yields an estimate of the true virial mass that is off by more than a factor two is smaller than 8 (2) percent in models with (without) feedback.

It is remarkable that the zero-point for models with feedback is the same as for models without feedback. Apparently, when matter is ejected it reduces V_{max} but at the same time increases the disc scale length such that $R_d V_{\text{max}}^2$ stays roughly constant, albeit with somewhat more scatter.

We therefore conclude that one can use equation (15) as a fairly reliable estimate of the total virial mass of disc galaxies.

In summary, contrary to naive expectations maximum rotation velocity and total luminosity are very poor indicators of the total virial mass. First of all the slope and zero-points of the $V_{\text{max}}(M_{\text{vir}})$ and $L_K(M_{\text{vir}})$ relations depend on the input parameters of the model. This means that an observer trying to infer M_{vir} from either V_{max} or L_K needs to make assumptions about the efficiencies of cooling and feedback. However, it is exactly these efficiencies that we seek to constrain. Secondly, the scatter of both relations can be so large that even if the normalization of the relation were known, one could still not infer M_{vir} to better than an order of magnitude. A much more reliable mass indicator is $R_d V_{\text{max}}^2 / G$, which can fairly easily be obtained from observations. Although the error in inferred virial mass for each individual galaxy can still exceed a factor two, especially when feedback is important, the *average* ratio between M_{vir} and $R_d V_{\text{max}}^2 / G$, averaged over a large ensemble of galaxies, is independent of the cooling and feedback efficiencies.

We now have all the tools in place to see whether we

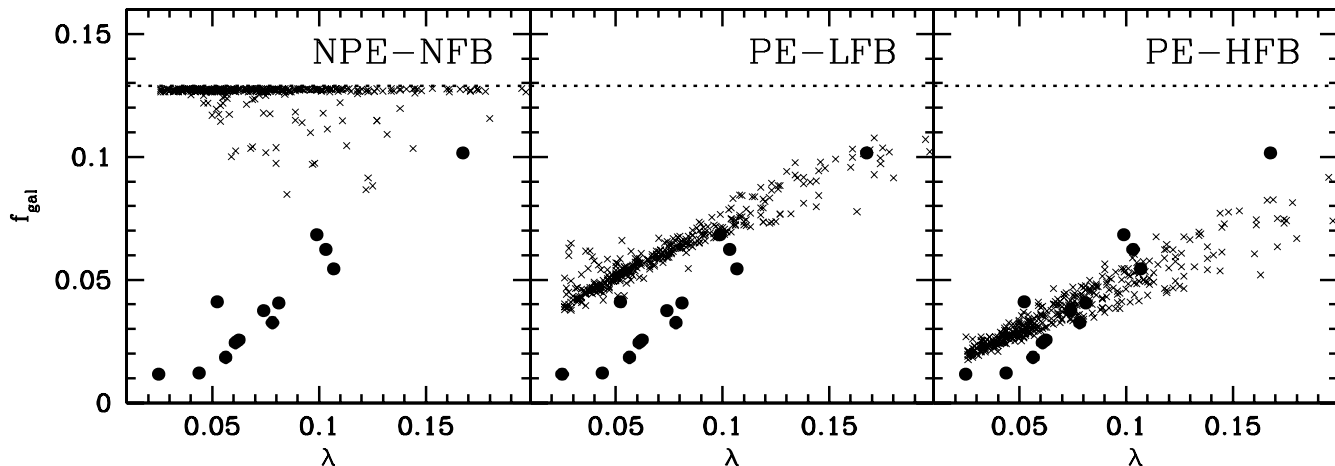


Figure 9. The relation between halo spin parameter λ and the galaxy mass fraction f_{gal} in models NPE-NFB, PE-LFB, and PE-HFB (crosses). The thick solid dots correspond to data on dwarf galaxy rotation curves analyzed by van den Bosch, Burkert & Swaters (2001). These data reveal a narrow correlation between f_{gal} and λ , which is reasonably well reproduced by the PE-HFB model. The model without feedback (NPE-NFB), on the other hand, predicts a clearly different relation between f_{gal} and λ . Note that here low values of f_{gal} are due to inefficient cooling rather than efficient feedback. This suggests that the low baryonic mass fractions of dwarf galaxies are due to feedback rather than inefficient cooling. See the text for a more detailed discussion.

can recover $f_{\text{gal}}(M_{\text{vir}})$ from the observables. Using $M_{\text{gal}} = M_{\text{cold}} + \Upsilon_B L_B$ with Υ_B given by equation (13), and using equation (15) to estimate M_{vir} we obtain the results plotted in Figure 8. This time we plot the results for all six models listed in Table 1. Crosses correspond to the true values of f_{gal} and M_{vir} , while the dots correspond to the values inferred from the observables as indicated above. In both models without feedback (PE-NFB and NPE-NFB) the scatter in the recovered $f_{\text{gal}}(M_{\text{vir}})$, which owes entirely to errors in the estimate of M_{vir} , is much larger than for the true values. Yet, the two models are sufficiently different to distinguish between them, and the estimates of f_{gal} nicely avoid the regions in the upper right corner which contains the information about the cooling efficiencies. In the models with feedback, the recovered values occupy roughly the same area of the $f_{\text{gal}} - M_{\text{vir}}$ plane as the intrinsic values. Although the one-to-one correspondence for individual model galaxies may be poor, statistically the method to recover $f_{\text{gal}}(M_{\text{vir}})$ explored here works remarkably well.

It is important to realize that the results shown in Figure 8 correspond to the idealized case. In reality there will be additional scatter from observational errors, from errors in estimates of the cold gas mass (which we have taken here to be known exactly), and from the unknown normalization of the relation between color and mass-to-light ratio due to uncertainties in the IMF. Nevertheless, despite this pessimistic outlook, there is still hope that the aforementioned method might at least be able to put some limits on the feedback efficiencies, as the resulting $f_{\text{gal}}(M_{\text{vir}})$ relation of the models with feedback clearly separates out from the two models without feedback. Although it will be extremely difficult to distinguish between medium and high feedback (i.e., models PE-MFB and PE-HFB), this is not a problem of the method, but owes mainly to the fact that even the intrinsic $f_{\text{gal}}(M_{\text{vir}})$ relations of these two models are fairly similar. This in turn reflects a saturation of the effective efficiency of feedback in expelling mass: stronger mass ejection

reduces the mass of new stars formed, which in turn reduces the mass ejection efficiency.

4.4 Correlations with halo spin parameter

The two main parameters that determine the characteristics of disc galaxies are the total mass and the halo spin parameter. So far we have focussed on $f_{\text{gal}}(M_{\text{vir}})$, and we discussed various indicators of M_{vir} . Here we turn our attention to $f_{\text{gal}}(\lambda)$.

In Figure 9 crosses plot the galaxy mass fractions as function of the halo spin parameter for models NPE-NFB, PE-LFB and PE-HFB. Only model galaxies with $50 \text{ km s}^{-1} \leq V_{\text{max}} \leq 150 \text{ km s}^{-1}$ are plotted. Models with and without feedback reveal a clearly different $f_{\text{gal}}(\lambda)$. In the latter, low values of f_{gal} are due to inefficient cooling, which is unrelated to the value of the spin parameter. However, in cases with feedback, a narrow correlation is evident whereby galaxies in low- λ haloes have lower galaxy mass fractions. This was already eluded to in Section 4.1, and is a result of the fact that haloes with less angular momentum produce higher surface brightness discs. Since the star formation efficiency is correlated with surface density (equation [7]) and the amount of ejected material is proportional to the amount of stars formed (equation [10]), systems with less angular momentum are more efficient in ejecting mass. Decreasing or increasing the feedback efficiency ε_{fb} moves the crosses up and down, respectively, but leaves the slope of the $f_{\text{gal}}(\lambda)$ relation intact. Therefore, if we could somehow measure both λ and f_{gal} we could use that to constrain the cooling and feedback efficiencies.

In principle, both the spin parameter of the baryons that make up the disc and the galaxy mass fraction can be determined from a detailed rotation curve analysis. In a recent study, van den Bosch, Burkert & Swaters (2001) applied such method to a sample of low mass disc galaxies (also with $50 \text{ km s}^{-1} \leq V_{\text{max}} \leq 150 \text{ km s}^{-1}$) for which accurate HI rotation curves and *R*-band photometry are available. Fitting

mass models to the observed rotation curves, van den Bosch et al. (2001) obtained estimates of both λ and f_{gal} which are plotted in Figure 9 as solid dots. Remarkably enough, these data points reveal a similarly narrow relation, albeit with a somewhat steeper slope, as our models with feedback. Taking these data point at face value thus suggests that the low baryonic mass fractions in dwarf galaxies are not due to inefficient cooling, but to efficient feedback.

However, it is important to realize that the values of λ plotted in Figure 9 correspond to the spin parameters of the dark matter haloes in the case of the model, but to that of the disc material (cold gas plus stars) in the case of the data. In the standard picture of disc formation (adopted in our models), the assumption is made that baryons conserve their specific angular momentum. Therefore, if all baryons end up in the disc, halo and disc should have the same spin parameter. However, since $f_{\text{gal}} \ll f_{\text{bar}}$ this clearly is not the case, implying that one can not simply compare the spin parameters of halo and disc. In fact, a straightforward interpretation of Figure 9 for the data seems to imply that discs form out of only a small fraction of the available baryons, but yet manage to draw most of the available angular momentum (see discussions in Navarro & Steinmetz 2000 and van den Bosch et al. 2001). However, the disc spin parameter is determined by integrating the ratio $M_{\text{disc}}(r)/M_{\text{disc}}(r_{\text{max}})$ over the entire disc (see van den Bosch et al. 2001). Here $M_{\text{disc}}(r)$ is the total disc mass inside radius r and r_{max} is the maximum extent of the disc. Therefore, λ_{disc} is still identical to λ_{halo} if, and only if, at each radius in the disc feedback has expelled an identical *fraction* of disc material. Surprisingly, as shown in paper 1, our simplistic feedback model establishes just that. Therefore, if feedback in the real Universe accomplishes a similar radial dependence, a direct comparison of model with data as in Figure 9 is justified.

Finally we emphasize that the errors on both f_{gal} and λ inferred from data can be quite significant (though hard to quantify). Both λ and f_{gal} are derived directly from the model fits to the observed rotation curves. However, as shown in van den Bosch & Swaters (2001), such mass models suffer from numerous uncertainties and degeneracies. For instance, inferring M_{vir} from the observed rotation curve, requires one to make assumptions regarding the density distribution of the dark matter halo (which sets the rotation curve shape), and cosmology (which sets the relation between virial mass and virial radius, the latter of which is required for the computation of λ). Furthermore, the scatter in the $f_{\text{gal}}(\lambda)$ relation of the model galaxies is also likely to be underestimated. For instance, the scatter in MAHs for a halo of given present day mass is likely to cause some scatter in the halo concentrations and the distributions of specific angular momentum, even for haloes with the same spin parameter (e.g., Jing 2000; Gardner 2001; van den Bosch 2001; Vitvitska et al. 2001; Wechsler et al. 2001), both of which will cause some additional scatter in the $f_{\text{gal}}(\lambda)$ relation. Since we adhere to the average, universal MAH and to the average halo concentration given by the model of Bullock et al. (2001c), this is not taken into account in the models. However, simple tests indicate that these effects are not very important, and furthermore, the scatter in the model galaxies is comparable to that of the data. This suggests that this technique might actually be able to provide meaningful constraints on feedback efficiencies, and it warrants a

more detailed exploration of the $f_{\text{gal}}(\lambda)$ relation for a larger sample of disc galaxies.

5 THE TULLY-FISHER RELATION

The fundamental scaling relation of disc galaxies, known as the Tully-Fisher (hereafter TFR) relation, couples the luminosities of disc galaxies to their rotation velocities. If light scales linearly with total galaxy mass, and rotation velocity with total virial mass, then the slope, scatter and zero-point of the TFR tell us directly about the efficiencies of cooling and feedback. Therefore, various authors in the past have used detailed models for the formation of disc galaxies to try and understand the origin of the TFR (e.g., Mo, Mao & White 1998; Avila-Reese & Firmani 2000; Firmani & Avila-Reese 2000; Mo & Mao 2000; van den Bosch 2000; Buchalter, Jimenez & Kamionkowski 2001). Although there is a general consensus that the TFR is governed by the relation between virial mass and circular velocity, it is still unclear what the observed TFR actually teaches us about cooling and feedback efficiencies. One of the main reasons for this lack of consensus is the discordant use of luminosity and rotation measures in TFRs. The slope and scatter of the TFR depend strongly on both photometric band and on whether one uses HI line widths or other measures of the galaxy's rotation velocity (e.g., Tully, Mould & Aaronson 1982; Pierce & Tully 1988; Gavazzi 1993; Courteau 1997; Verheijen 2001). This emphasizes that it is of crucial importance to extract the proper ‘observables’ from the models when comparing them to data, something that is often ignored. An additional reason why the interpretation of the TFR is still heavily debated is related to the fact that luminosity and rotation velocity not necessarily scale linearly with galaxy mass and virial mass, respectively. For example, as shown in Section 4 these naive expectations are not fulfilled in our models. This implies that the characteristics of the TFR become sensitive to the more subtle details of the models, which can differ substantially from one researcher to the other.

In Figure 10 we plot the present day K -band TF relations for our six models. We choose the K -band since it is less susceptible to uncertainties related to stellar population modeling and dust extinction. The solid and dashed lines in each panel correspond to TF relations of the form

$$L_k = b \left(\frac{V_{\text{max}}}{100 \text{ km s}^{-1}} \right)^a \quad (16)$$

and are plotted for comparison. The solid lines correspond to the TF relation of the RC/FD sample of Ursa Major cluster galaxies of Verheijen (2001) for which $a = 4$ and $b = 6.19 \times 10^9 L_{\odot}$. The dashed lines correspond to a fiducial TF relation with $a = 3$ normalized to the TF relation of Verheijen at $V_{\text{max}} = 100 \text{ km s}^{-1}$. Although we have in no way attempted to fit our models to reproduce any observed TFR, it is reassuring that our zero-points are in reasonable agreement with the empirical TF relation of Ursa Major cluster galaxies. In the PE-NFB model the TFR has a slope $a \simeq 4$. Although the scatter in V_{max} at given M_K is fairly large, it is significantly smaller than the scatter in V_{max} at given M_{vir} shown in Figure 7: more compact discs have relatively higher V_{max} , but at the same time convert a larger

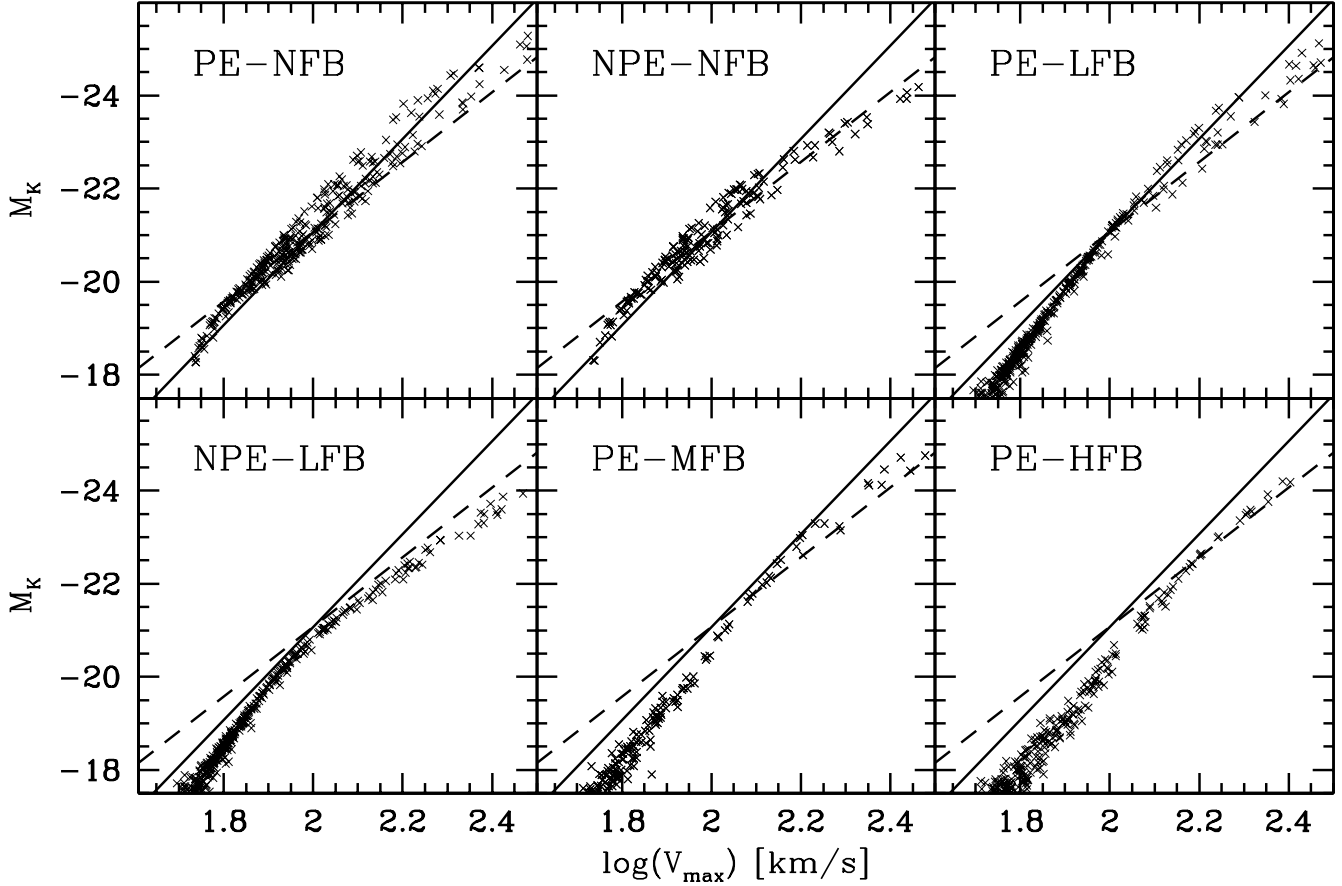


Figure 10. *K*-band Tully-Fisher relations for the six models listed in Table 1. Crosses correspond to the model galaxies, while the solid (dashed) lines correspond to TFRs of the form $L_K \propto V_{\max}^a$ with $a = 4$ ($a = 3$), and are plotted for comparison. In fact, the solid lines correspond to the observed TF relation of Verheijen (2001), while the dashed lines correspond to a fiducial TF relation with $a = 3$ with the zero-point normalization of Verheijen (2001) at $V_{\max} = 100 \text{ km s}^{-1}$. Note how most of the models predict some amount of curvature in the TFR, steepening from $a \simeq 3$ at the bright end to $a \simeq 4$ at the faint end. See the text for a detailed discussion.

fraction of their gas into stars, and are therefore brighter. Variation in λ therefore partially scatters galaxies with identical M_{vir} along the TFR, rather than perpendicular to it (see also van den Bosch 2000). The introduction of feedback helps to further suppress the amount of scatter in the TFR, as its mass ejection efficiency is strongly correlated with λ (cf. Section 4.4).

More importantly, introducing feedback or reducing the cooling efficiencies both introduce a curvature in the TFR; the luminous end of the TFR has a slope $a \simeq 3$, which steepens to $a \simeq 4$ towards lower luminosities. If the true TFR reveals a similar behavior than (i) the observed slope of the TFR depends strongly on the sample of galaxies used (i.e., on the relative number of bright and faint galaxies), and (ii) it will be impossible to distinguish between efficient feedback and inefficient cooling based on the TFR alone. Furthermore, the TFR contains very little information about the actual feedback efficiency (i.e., compare models PE-LFB, PE-MFB, and PE-HFB). Increasing ε_{fb} lowers both V_{\max} and L_K , such that it mainly shifts model galaxies along the TFR (see also Mo & Mao 2000). We therefore conclude that the TFR not necessarily provides the most useful constraint on theories of disc formation (but see Shen, Mo & Shu 2001 for a possible way of breaking these various de-

generacies). Secondly, the results shown here indicate that it is extremely useful to obtain a TFR that spans as large a range in luminosities as possible, for only then can one conclusively infer whether or not the TFR reveals a curvature (i.e., most observed TF relations only probe down to $V_{\max} \simeq 100 \text{ km s}^{-1}$).

6 STAR FORMATION RATES, COLORS AND METALLICITIES

As we have shown in Section 3.1, the star formation rates of disc galaxies are largely governed by the rate at which the galaxies accrete mass. Therefore, one might hope to be able to reconstruct the mass accretion history of disc galaxies from observations of their star formation rate as function of redshift. However, the efficiencies of cooling and feedback will influence the strength of the coupling between mass accretion and star formation. In order to investigate how strong these effects are we compute the average star formation rate (averaged over all model galaxies in each sample) for each of the models listed in Table 1. Results are shown in Figure 11 (thin lines). For comparison, we also plot (as a thick solid line) the average mass accretion rate, which

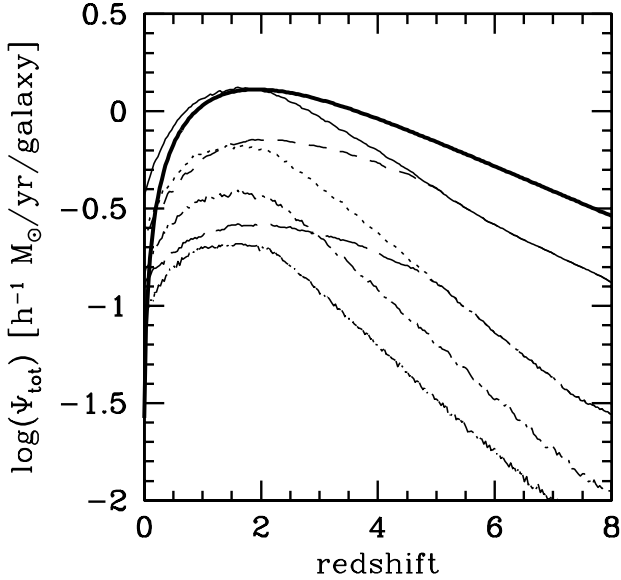


Figure 11. The average star formation rates (averaged over all galaxies in each sample) as function of redshift. The various thin lines correspond to the six models: PE-NFB (thin solid line), NPE-NFB (short-dashed line), NPE-LFB (long-dashed line), PE-LFB (dotted line), PE-MFB (short-dash – dotted line), and PE-HFB (long-dash – dotted line). The thick solid line corresponds to the average *mass* accretion rate, lowered by a factor ten to facilitate a comparison with the star formation rates. Note how small changes in the feedback and cooling efficiencies impact strongly on the star formations rates.

is identical for all six models. Although to zeroth order the overall shapes of the star formation histories are similar to that of the mass accretion history, the SFHs are strongly model dependent. First of all, the absolute values of the SFR depends strongly on the feedback efficiency: for example, the SFR in the PE-HFB model with $\varepsilon_{fb} = 0.1$ is an order of magnitude lower than for the PE-NFB model without feedback. Secondly, reducing the metallicity of the hot gas impacts strongly on the SFRs: the ‘no pre-enrichment’ models NPE-NFB and NPE-LFB both yield much lower SFRs at low redshift than models PE-NFB and PE-LFB, respectively, in which the hot gas is pre-enriched to one-third Solar. Finally, whereas the mass accretion rate drops rapidly for $z \lesssim 1$, the decrease in the SFR is much less dramatic. This reflects a weakness of the coupling between mass accretion and star formation. Even after mass accretion is completely quenched, cold gas in the disc can still continue to form stars, and hot gas in the halo still continues to cool and provide new material for star formation to the disc. These results clearly show that the ‘cosmic star formation history’ (Lilly et al. 1996; Madau, Pozzetti & Dickinson 1998) not only depends on cosmology (which sets the halo mass accretion histories), but also on details related to the cooling and feedback efficiencies, making an interpretation of the cosmic star formation history highly degenerate.

In addition to the star formation rates, variations in cooling and feedback efficiencies also impact on the chemical enrichment history. Such effects should be observable through the colors and metallicities of the galaxies. In Fig-

ure 12 we plot some results for three representative models: PE-NFB, PE-LFB, NPE-LFB (see Table 1).

The upper panels of Figure 12 plot the present day metallicity of the cold gas in the disc as function of the absolute *K*-band magnitude. All models reveal a clear metallicity-luminosity relation in which brighter galaxies have higher (gas) metallicities. In models with feedback, this owes largely to the fact that more massive systems are more efficient in retaining the metals. In the PE-NFB model no feedback is included, but yet the brighter galaxies are more enriched. This is a consequence of the star formation threshold density, which induces larger gas mass fractions in less massive systems (cf. Figure 5). The metallicity-luminosity relations of the various models are sufficiently different that there is hope that the observed relation might help to constrain models of disc formation. In particular, in the NPE-LFB model faint galaxies have extremely low metallicities. Such galaxies are absent in models in which the hot gas is pre-enriched, and metallicities of low luminosity dwarf galaxies should therefore in principle allow to put limits on the amount of pre-enrichment. However, the details of our results depend clearly on the IRA used and on the value of the stellar yield (which depends on the IMF). Unless a more realistic chemical enrichment model is used, and we can independently constrain the stellar yield, we therefore remain skeptical that the observed metallicity-luminosity relation can place stringent constraints.

The panels in the middle row of Figure 12 plot the ratio $\Psi(0)/\Psi(1)$ of the present day SFR to that at $z = 1.0$. In the PE-NFB model there is a smooth trend running from $\Psi(1) \simeq 0.1\Psi(0)$ at the faint end to $\Psi(1) \simeq \Psi(0)$ for the brightest galaxies. This is a direct reflection of the mass dependence of the MAH: less massive systems form earlier, and therefore reveal a declining star formation rate for $z \lesssim 1$, while more massive systems form later and are still actively forming stars today. In the two models with feedback (PE-LFB and NPE-LFB) there is a large amount of scatter in $\Psi(0)/\Psi(1)$ for faint galaxies. This scatter is not related to the scatter in halo spin parameters, but rather reflects the semi-stochastic star formation history of these systems: after the onset of star formation, feedback ejects a significant fraction of the cold gas, lowering the surface density of the gas to below the star formation threshold level. Consequently, star formation is quenched until enough new gas has cooled that new stars can form. This ‘feedback’-loop causes the SFRs to fluctuate wildly with time, which reflects itself in a large amount of scatter in $\Psi(0)/\Psi(1)$.

The luminosity dependence of the star formation histories impacts directly on the color-magnitude diagrams of the resulting galaxies, which are plotted in the lower panels of Figure 12. Since the more massive systems form their stars relatively late, their stellar populations are relatively younger, and thus bluer. This is opposite to the observed trend, in which faint galaxies are bluer than bright galaxies (e.g., Gavazzi 1993; Fioc & Rocca-Volmerange 1999; Schombert, McGaugh & Eder 2001). This is shown by the solid line which corresponds to the color magnitude relation derived by van den Bosch & Dalcanton (2000). These authors compiled *B* and *K* band magnitudes from the literature for a sample of 139 spiral galaxies of type Sb or later, spanning the magnitude interval $-16 \lesssim M_K \lesssim -26$, and corrected these for external extinction.

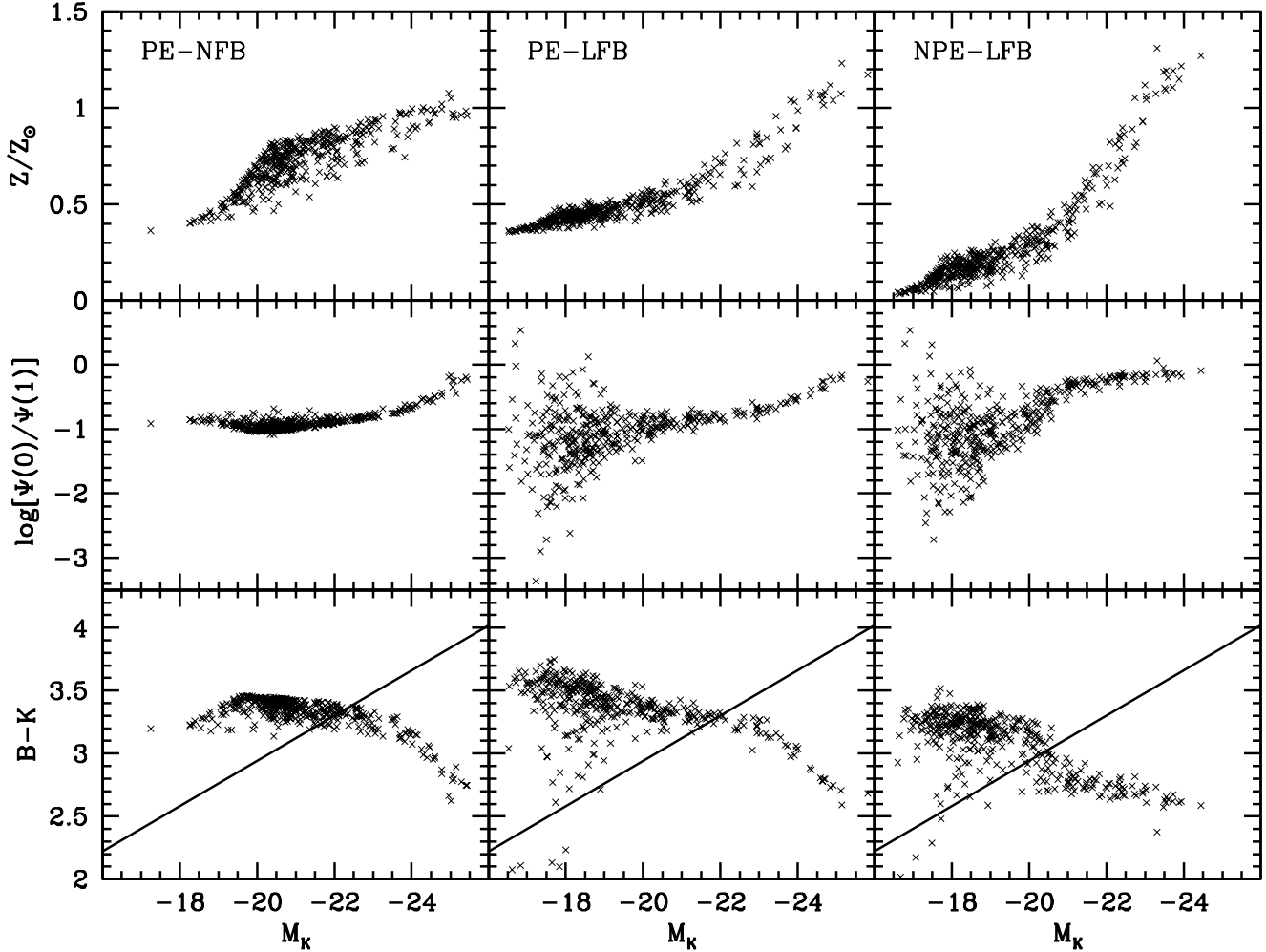


Figure 12. The upper panels plot the present day metallicity of the cold gas (in units of solar metallicity) as function of absolute K -band magnitude for three representative models. In all cases there is a clear correlation in which brighter galaxies have higher metallicities. In the models with feedback (PE-LFB and NPE-LFB) this owes mainly to the fact that more massive galaxies are more efficient at retaining metals (i.e., less ejection). In the model without feedback, this reflects the higher efficiency of more massive systems to turn their cold gas into stars (i.e., more enrichment). The panels in the middle row plot the ratio of the present day SFR to that at $z = 1$. In the PE-NFB model there is a narrow correlation with M_K , reflecting the mass dependence of the MAHs of dark matter haloes. In the models with feedback star formation is semi-stochastic, causing a large spread in $\Psi(0)/\Psi(1)$ for faint galaxies. Bottom panels plot the present day $B - K$ color versus K -band magnitude. The solid lines correspond to the observed color-magnitude relation (van den Bosch & Dalcanton 2000). Our models clearly fail to reproduce the observed color-magnitude relation of disk galaxies. In fact, the models reveal an inverted relation, with more luminous galaxies becoming bluer (see discussion in text).

Introducing feedback only aggravates the problem: the SN induced mass ejection quenches later star formation, thus producing faint galaxies that are extremely red. Only a small fraction of the dwarf galaxies in the PE-LFB and NPE-LFB models have sufficiently low values of $\Psi(0)/\Psi(1)$ that their $B - K$ color is as blue as observed. Even extremely strong metallicity-luminosity relations, such as in the NPE-LFB model, can not reverse the color-magnitude relation which is completely dominated by the mass dependence of the star formation histories. Even though faint galaxies in the NPE-LFB model are significantly bluer than in the PE-LFB model (because they have lower metallicities), they are still redder than their more luminous counterparts. This indicates a generic problem for any hierarchical picture of galaxy formation in which more massive systems form later.

A similar problem, but for early-type galaxies, has been identified in semi-analytical models of galaxy formation (e.g., Kauffmann et al. 1993; Baugh, Cole & Frenk 1996; Cole et al. 2000). Kauffmann & Charlot (1998) have shown that this problem can be solved when strong feedback is included in the models, inducing a strong mass-metallicity relation. However, as is evident from the NPE-LFB model, this does not work for disk galaxies. The reason is that early-type galaxies have much older stellar populations than disk galaxies. A difference between 3 and 5 Gyrs implies a much stronger color difference than one between 8 and 12 Gyr. Consequently, in disk galaxies, which have relatively young stellar populations, the mass-metallicity relation is not strong enough to invert the color-magnitude relation.

Therefore, the color-magnitude relation problem is more severe for late-type galaxies than for early-type galaxies.

Part of the problem may be solved by including dust in the models. Since more massive systems have higher metallicities, it is likely that they contain more dust, and should therefore be relatively more reddened than faint galaxies. However, the problem is not only that bright galaxies are too blue (which might be solved by including dust extinction), but also that the faint galaxies are too red. We intend to return to this intriguing problem in a future paper. For the moment we emphasize that variations in cooling and feedback efficiencies do leave signatures in the metallicities and colors of galaxies, but that there is little hope to use observations to constrain these efficiencies before we have a better understanding of the observed color-magnitude relations of disc galaxies.

7 CONCLUSIONS

Currently the largest uncertainties in galaxy formation modeling are related to the efficiencies of cooling, feedback and star formation. In particular, we need to understand how these efficiencies regulate what fractions of available baryons are converted into luminous matter, what fractions are ejected out of the dark matter haloes by feedback processes, and what fractions remain in the hot phase because of inefficient cooling. These efficiencies are expected to depend on both the mass and angular momentum of the protogalaxies. Therefore, if we can somehow determine the total virial mass and angular momentum of galaxies from observations of their luminous component this allows us to put stringent constraints on the baryonic physics that play an important role in the process of galaxy formation.

In this paper we used models for the formation of disc galaxies presented by van den Bosch (2001) to investigate which observables, extracted directly from those models, are best suited to constrain the initial conditions (i.e., mass and angular momentum) of the protogalaxies. Rather than attempting to fit the models to real data, we examined how variations in the efficiencies of cooling and feedback impact on the models. The models assume that dark matter haloes grow smoothly in mass (no mergers) with a rate that depends on cosmology. Inside the virialized haloes gas cools and conserves its angular momentum (which owes from cosmological torques), thus settling in a disc component. No a priori assumption is made regarding the density distribution of the disc. The models take star formation, bulge formation, chemical evolution, and mass ejection due to energy input from SNe (feedback) into account, and output masses (of six different components), luminosities (in various photometric bands), rotation velocities, and metallicities as functions of both time and galactocentric radius.

The two main parameters that we varied in this paper are the metallicity of the gas prior to cooling (which sets the cooling efficiency) and the fraction of SN energy that is used to drive mass outflow (which sets the feedback efficiency). These two parameters strongly impact on the galaxy mass fraction f_{gal} , defined as the fraction of total virial mass that is part of the galaxy (disc plus bulge), and in particular on how f_{gal} depends on virial mass and halo spin parameter. Therefore, if observations could somehow determine

$f_{\text{gal}}(M_{\text{vir}}, \lambda)$ it would place strong constraints on theories of galaxy formation. We therefore examined which of the observables extracted directly from the models are best suited to reconstruct $f_{\text{gal}}(M_{\text{vir}}, \lambda)$ without prior knowledge of the feedback and cooling efficiencies. The main challenge is to find a proper mass estimator of M_{vir} . We have shown that both V_{max} (the maximum of the galaxy's rotation curve) and total luminosity are poor indicators of M_{vir} : the scatter of the $V_{\text{max}}(M_{\text{vir}})$ and $L_K(M_{\text{vir}})$ relations can be extremely large, while at the same time the slope and zero-points of the relations depend on the actual model input parameters. A much more reliable mass indicator is $R_d V_{\text{max}}^2 / G$, which can fairly easily be obtained from observations. Although the error in inferred virial mass for each individual galaxy can still exceed a factor two, especially when feedback is important, we find the *average* ratio between M_{vir} and $R_d V_{\text{max}}^2 / G$, averaged over a large ensemble of galaxies, to be independent of the cooling and feedback efficiencies. In fact, we have shown that with this estimator of the total virial mass, we can recover the intrinsic $f_{\text{gal}}(M_{\text{vir}})$ accurately enough to distinguish between the various models.

Given the difficulties with determining M_{vir} many studies in the past have studied the direct relation between luminosity and rotation velocities, known as the Tully-Fisher relation, to try and constrain galaxy formation. Most of the models presented in this paper reveal TFRs that are curved: they change from $L \propto V_{\text{max}}^3$ at the bright end to $L \propto V_{\text{max}}^4$ at the faint end. In order to detect such curvature observationally it is essential that one obtains data that spans as wide a range in luminosities as possible. Furthermore, even if such curvature is detected, there is little hope that one can distinguish between effective feedback and ineffective cooling, both of which leave similar features in the slope and scatter of the TFR. Although our models are probably not completely realistic, this suggests that the TFR does not necessarily provide the most useful constraints on disc galaxy formation.

Another approach that has been taken in the past, is to use published luminosity functions and luminosity-velocity relations to construct halo velocity functions (i.e., Shimasaku 1993; Newman & Davis 2000; Gonzales et al. 2000; Bullock et al. 2001a; Kochanek 2001). The main goal of these studies is similar to the work presented here, namely to circumvent the problems with poorly understood astrophysical processes when linking the observed properties of galaxies to those of their dark matter haloes. Our results imply that great care is to be taken in linking an observable velocity such as V_{max} to the circular velocity of a dark matter halo (see also discussions in Gonzales et al. 2000 and Kochanek 2001). Based on our results, we suggest that the construction of a halo *mass* function using $M_{\text{vir}} \propto R_d V_{\text{max}}^2$ may prove more reliable.

In the absence of feedback f_{gal} depends only on halo mass and is independent of the halo angular momentum. However, when feedback is included f_{gal} correlates strongly with the halo spin parameter λ (at least for the less massive systems). Systems with less angular momentum produce discs with higher surface brightness, which have higher star formation rates, and consequently also higher mass ejection rates. Therefore, if we could somehow determine the halo spin parameter, we could use its correlation with f_{gal} (or absence thereof), to constrain the efficiencies of feedback pro-

cesses. In a recent study van den Bosch, Burkert & Swaters (2001) used high quality rotation curve data for a sample of dwarf galaxies to construct $f_{\text{gal}}(\lambda)$. Interestingly, they found a narrow correlation with f_{gal} decreasing with decreasing λ , as predicted by our models. Although it is tempting to interpret this as evidence that feedback does play an important role in disc galaxy formation, there are several problems. First of all, the slope of the ‘observed’ $f_{\text{gal}}(\lambda)$ relation is steeper than predicted by the model. Secondly, the spin parameter of the disc material (which is the one obtained from the observations) is not necessarily the same as that of the dark matter halo. Finally, there are various uncertainties related to obtaining estimates of both λ and f_{gal} from the rotation curve analysis that may cause systematic errors. Nevertheless, the small amount of scatter in $f_{\text{gal}}(\lambda)$ in both the model predictions and the data suggests that a similar analysis as in van den Bosch, Burkert & Swaters for a larger sample of galaxies may prove extremely useful for constraining the feedback efficiencies.

The structural properties of present day disc galaxies (scale length, disc-to-bulge ratio, gas mass fraction, rotation velocities) depend mainly on mass and angular momentum. They contain virtually no information about the mass accretion history (MAH) of the galaxy, which mainly determines the current and past star formation rates. Therefore, one might hope to be able to use the observed cosmic star formation history of disc galaxies to infer the overall MAH of dark matter haloes, which can be used to constrain cosmological parameters. However, as we have shown, small changes in the feedback and cooling efficiencies impact strongly on the star formation histories. In fact, many different combinations of cosmology, feedback, and cooling efficiency can produce similar star formation histories, which implies that the interpretation of the cosmic star formation history is highly degenerate.

Finally we investigated how cooling and feedback influence the colors and metallicities of the model galaxies. In models with feedback, more luminous systems are more efficient in retaining metals, producing a fairly narrow metallicity-luminosity relation. Surprisingly, also in models without feedback the more luminous galaxies are more enriched. This owes to the star formation threshold density, due to which more massive systems can convert a larger fraction of their gas into stars, causing more enrichment. Contrary to observations, we find color-magnitude relations in which brighter galaxies are bluer. This is a consequence of the hierarchical nature of structure formation, in which more massive structures form later. Since star formation rates are mainly driven by the rate at which galaxies accrete mass, more luminous galaxies end up with relatively younger stellar populations. Even though the more luminous galaxies have substantially higher metallicities (which tends to make them redder), the differences in stellar population ages dominates, and causes brighter galaxies to be bluer. It remains to be seen whether more sophisticated modeling of the chemical enrichment and feedback processes, combined with a treatment of dust extinction can solve this intricate problem.

ACKNOWLEDGEMENTS

I am grateful to Anthony Brown, Guinevere Kauffmann, Houjun Mo, Chenggang Shu, and Simon White for suggestions, advice and stimulating discussions, and to the anonymous referee for insightful comments that helped to improve the paper.

REFERENCES

- Avila-Reese V., Firmani C., 2000, *RevMexAA*, 36, 23
- Balogh M.L., Pearce F.R., Bower R.G., Kay S.T., 2001, *MNRAS*, 326, 1228
- Barnes J.E., Efstathiou G., 1987, *ApJ*, 319, 575
- Baugh C.M., Cole S., Frenk C.S., 1996, *MNRAS*, 283, 1361
- Bell E.F., de Jong R.S., 2001, *ApJ*, 550, 212
- Blumenthal G.R., Faber S.M., Flores R., Primack J.R., 1986, *ApJ*, 301, 27
- Bond J.R., Cole S., Efstathiou G., Kaiser N., 1991, *ApJ*, 379, 440
- Bryan G., Norman M., 1998, *ApJ*, 495, 80
- Bruzual G.A., Charlot S., 1993, *ApJ*, 405, 538
- Buchalter A., Jimenez R., Kamionkowski M., 2001, *MNRAS*, 322, 43
- Bullock J.S., Dekel A., Primack J.R., Somerville R.S., 2001a, *ApJ*, 550, 21
- Bullock J.S., Dekel A., Kolatt T.S., Kravtsov A.V., Klypin A.A., Porciani C., Primack J.R., 2001b, *ApJ*, 555, 240
- Bullock J.S., Kolatt T.S., Sigad Y., Somerville R.S., Klypin A.A., Primack J.R., Dekel A., 2001c, *MNRAS*, 321, 559
- Burton W.B., Gordon M.A., 1978, *A&A*, 63, 7
- Christodoulou D.M., Shlosman I., Tothline J.E., 1995, *ApJ*, 443, 551
- Cole S., Lacey S., 1996, *A&A*, 281, 716
- Cole S., Lacey C.G., Baugh C.M., Frenk C.S., 2000, *MNRAS*, 319, 168
- Courteau S., 1997, *AJ*, 114, 2402
- Fardal M.A., Katz N., Gardner J.P., Hernquist L., Weinberg D.H., Davé R., 2001, *ApJ*, 562, 605
- Fioc M., Rocca-Volmerange B., 1999, *A&A*, 351, 869
- Firmani C., Avila-Reese V., 2000, *MNRAS*, 315, 457
- Flores R., Primack J.R., Blumenthal G.R., Faber S.M., 1993, *ApJ*, 412, 443
- Gardner J.P., 2001, *ApJ*, 557, 616
- Gavazzi G., 1993, *ApJ*, 419, 469
- Gonzales A.H., Williams K.A., Bullock J.S., Kolatt T.S., Primack J.R., 2000, *ApJ*, 528, 145
- Katz N., Weinberg D.H., Hernquist L., 1996, *ApJS*, 105, 19
- Kauffmann G., Charlot S., 1998, *MNRAS*, 297, 23
- Kauffmann G., White S.D.M., Guiderdoni B., 1993, *MNRAS*, 264, 201
- Kay S.T., Pearce F.R., Frenk C.S., Jenkins A., 2001, preprint (astro-ph/0106462)
- Kennicutt R.C.Jr., 1989, *ApJ*, 344, 685
- Kennicutt R.C.Jr., 1998, *ApJ*, 498, 541
- Kochanek C.S., 2001, preprint (astro-ph/0108160)
- Lacey C., Cole S., 1993, *MNRAS*, 262, 627
- Lilly S.J., Le Fevre O., Hammer F., Crampton D., 1996, *ApJ*, 460, L1
- Madau P., Pozzetti L., Dickinson M., 1998, *ApJ*, 498, 106
- Mo H.J., Mao S., White S.D.M., 1998, *MNRAS*, 295, 319
- Mo H.J., Mao S., 2000, *MNRAS*, 318, 163
- Mushotzky R., Loewenstein M., 1997, *ApJ*, 481, 63
- Natarajan P., 1999, *ApJ*, 512, 105
- Navarro J.F., Frenk C.S., White S.D.M., 1997, *ApJ*, 490, 493
- Navarro J.F., Steinmetz M., 2000, *ApJ*, 538, 477
- Newman J.A., Davis M., 2000, *ApJ*, 534, L11

- Pearce F.R., Thomas P.A., Couchman H.M.P., Edge A.C., 2000, MNRAS, 317, 1029
- Pierce M.J., Tully R.B., 1988, ApJ, 330, 579
- Press W., Schechter P., 1974, ApJ, 187, 425
- Ryden B.S., 1988, ApJ, 329, 589
- Scalo J.N., 1986, Fundam. Cosmic Phys., 11, 1
- Schmidt M., 1959, ApJ, 129, 243
- Schombert J.M., McGaugh S.S., Eder J.A., 2001, AJ, 121, 2420
- Shen S., Mo H.J., Shu C., 2001, preprint (astro-ph/0105095)
- Sheth R.K., Tormen G., 1999, MNRAS, 308, 119
- Shimasaku K., 1993, ApJ, 413, 59
- Silk J., 1997, ApJ, 481, 703
- Simien F., de Vaucouleurs G., 1986, ApJ, 302, 564
- Somerville R.S., Primack J.R., 1999, MNRAS, 310, 1087
- Sutherland R., Dopita M., 1993, ApJS, 88, 253
- Toomre A., 1964, ApJ, 139, 1217
- Tóth G., Ostriker J.P., 1992, ApJ, 389, 5
- Tully R.B., Mould J., Aaronson M., 1982, ApJ, 257, 527
- Tytler D., Burles S., Lu L., Fan X.-M., Wolfe A., Savage B., 1999, AJ, 117, 63
- van Albada T.S., Bahcall J.N., Begeman K., Sancisi R., 1985, ApJ, 295, 305
- van den Bosch F.C., 1998, ApJ, 507, 601
- van den Bosch F.C., 2000, ApJ, 530, 177
- van den Bosch F.C., 2001, MNRAS, 327, 1334 (paper 1)
- van den Bosch F.C., 2002, MNRAS, in press (astro-ph/0105151)
- van den Bosch F.C., Dalcanton J.J., 2000, ApJ, 534, 146
- van den Bosch F.C., Swaters R.A., 2001, MNRAS, 325, 1017
- van den Bosch F.C., Burkert A., Swaters R.A., 2001, MNRAS, 326, 1205
- Verheijen M.A.W., 2001, ApJ, in press (astro-ph/0108225)
- Vitvitska M., Klypin A.A., Kravtsov A.V., Bullock J.S., Wechsler R.H., Primack J.R., 2001, preprint (astro-ph/0105349)
- Warren M.S., Quinn P.J., Salmon J.K., Zurek W.H., 1992, ApJ, 399, 405
- Wechsler R.H., Bullock J.S., Primack J.R., Kravtsov A.V., Dekel A., 2001, preprint (astro-ph/0108151)
- White S.D.M., Rees M.J., 1978, MNRAS, 183, 341